

CYCLOTRON RADIATION FROM ELECTRON STREAMS AS THE ORIGIN OF SOLAR TYPE I NOISE STORMS

By P. C. W. FUNG* and W. K. YIP*

[*Manuscript received May 26, 1966*]

Summary

In this report, cyclotron radiation from electron streams gyrating in some spot-field configurations in the corona is proposed to be the origin of solar type I noise storm radiation. In order to investigate whether one or both of the characteristic waves (ordinary and extraordinary modes) will carry significant electromagnetic energy and be observed, we study, for two characteristic modes, the power spectra from single electrons, the process of amplification of electromagnetic waves in a stream-plasma system, the power loss due to harmonic resonance absorption, and the escape conditions. It is found that in most cases the radiation in the o-mode is predominant. With two types of solutions in the simultaneous solution of the Appleton-Hartree equation and the Doppler equation, both the occurrence of narrow-band burst emissions and wide-band continuum radiation can be explained by the cyclotron generating mechanism. Moreover, many of the observed features are found to agree well with the predictions of the theory.

I. INTRODUCTION

During solar disturbed periods, the most common radio events on metre waves are the occurrences of type I radio emissions or type I "noise storms". This type of radiation consists of a slowly varying, broad-band emission (called "background continuum") lasting up to hours or days, on which are superimposed series of intense, narrow-band, short-lived bursts (called "storm bursts"). The radiation is usually strongly circularly polarized and its occurrence is always associated with a sunspot group. Even though this common non-thermal radiation has been observed since 1942 (e.g. Hey 1946; Martyn 1946; Pawsey 1950), the theoretical interpretations of this complex phenomenon so far published have been unsatisfactory. Before we put forward a theory to explain this type of solar emission, we will summarize the important observed features below.

(i) *Bandwidth*

The bandwidth of background continuum radiation usually extends to 100 Mc/s while that of a burst is very narrow, typically around 4 Mc/s (Payne-Scott, Yabsley, and Bolton 1947; Wild 1951; Elgaroy 1961). However, wide-band bursts having bandwidths up to 35 Mc/s have been observed less frequently (Vitkevich and Gorelova 1961).

(ii) *Relation Between the Occurrence of Background Continuum and that of Storm Bursts*

- (1) There is good general daily correlation between the occurrences of the two components (Fokker 1960). However, during some periods a strong con-

* Physics Department, University of Tasmania, Hobart.

tinuum radiation is detected with no appreciable burst emission, and vice versa (Wild 1951).

- (2) There is no apparent correspondence between the integrated spectrum of bursts and the observed spectrum of continuum radiation (Fokker 1960).

(iii) *Polarization* (Suzuki 1961; Kai 1962)

- (1) Referring to the magnetic polarity of the stronger member (normally the preceding spot) of a sunspot group, in most cases the polarization of both background continuum and bursts corresponds to the ordinary-mode radiation in the magnetoionic theory. The senses of polarization of both storm bursts and background continuum at an instant during a noise storm are the same.
- (2) The majority of storm bursts are close to 100% circularly polarized. However, sometimes there are noise storms that are composed of partially polarized, mixed polarized, or completely unpolarized bursts. A partially polarized storm occurs very often near the limb. There is also a tendency that the percentage polarization of the storm correlating to one spot group decreases rather suddenly at the limb.

(iv) *Apparent Source Positions* (Fokker 1960; Suzuki 1961; Kai 1962)

- (1) The experimental result on apparent storm centres, as observed on the Earth with respect to the position on the solar disk, indicates that the number of occurrences of noise storms decreases from the central meridian towards the limb. This means that the storm radiation has a narrow directivity.
- (2) In general, the observed frequency of a noise storm decreases with increasing apparent source height.
- (3) Morimoto and Kai (1961) investigated statistically the heights of type I bursts on 200 Mc/s from a comparison of the corresponding optical phenomena. The mean height of the source was found to be about $0.2R_0$ (R_0 = solar radius) above the photosphere near the centre of the disk and to increase towards the limb.
- (4) Perhaps the most interesting result in position observation is that storm centres are located near, but slightly above, the corresponding plasma levels of the $10 \times$ Baumbach-Allen model (Kundu 1964; Weiss, unpublished data).

(v) *Association of Occurrence of Noise Storms with Solar Flares and Sunspots*

- (1) Most noise storms are received within 2 hr after the occurrence of a flare and the most probable delay time between noise storms and flares is found to be approximately 30 min. However, simultaneous occurrence of a noise storm and a flare has been observed (Wild 1951; Fokker 1960).
- (2) Noise storms are always associated with a sunspot group when the maximum area of the group is greater than about 6×10^{-4} of the solar disk and when the maximum area of the largest spot in the group is greater than about

4×10^{-4} of the solar disk. For sunspots of areas greater than 7.5×10^{-4} of the solar disk, the probability of association between the occurrence of noise storms and sunspots increases with the maximum magnetic field strength associated with the spots (Payne-Scott and Little 1951; Malinge 1963).

(vi) *Angular Size of Apparent Storm Centres*

- (1) Tchichachev (1956) and Fokker (1960) observed that the storm centres on 200 Mc/s occupy diameters between 4 and 7 min of arc, while storm centres on 150 Mc/s have an average size of 8'. The fact that the average source size of a noise storm decreases with increasing frequency has also been observed by Wild and Sheridan (1958).
- (2) The angular sizes of storm bursts were found to be much smaller than those of storm centres, being less than 1'.6 on 105–140 Mc/s (Goldstein 1959).
- (3) The size of the background continuum in a noise storm has been found to be the same as the scattering range of the individual bursts (Kai 1962).

For other observed properties, such as the duration, frequency drift nature of storm bursts, and flux density received, the reader is referred to the comprehensive review of the subject contributed by Kundu (1964).

To explain part of the stated observed properties, a number of theories concerning the generating mechanism and propagation conditions have been proposed (Kiepenheuer 1946; Kruse, Marshall, and Platt 1956; Takakura 1956, 1963; Twiss and Roberts 1958; Denisse 1959*a*, 1959*b*; Ginzburg and Zheleznyakov 1959, 1961; Malinge 1963). However, all these theories have been speculative only. Each theory is successful in explaining a few aspects of the observed properties. To put forward a successful theory, one has to study the theory in great detail, in a quantitative way. Indeed, among all types of solar emissions, type I noise storms occur most frequently during solar active periods. Knowledge of the generating mechanism and propagation conditions will lead to a much better understanding of the physical conditions in the solar corona, particularly during the active periods. We intend, therefore, to investigate the cyclotron radiation theory and the propagation of the subsequent electromagnetic waves in detail.

We suggest that cyclotron radiation from electron streams gyrating in spot-field configurations is the cause of both the background continuum and the burst radiation. In Section II we set up models for the corona density distribution and some forms of spot-field configurations. In Section III, we study the possible emitted range of frequencies for ordinary modes (o-modes) and for extraordinary modes (x-modes) by assuming some pitch angles and kinetic energies of the electrons spiralling along the spot magnetic fields. The Eidman equation* is employed to investigate the power spectrum radiated by a single electron in a magnetoactive plasma (corona) for both modes. From a radiative instability theory developed by Fung (1966*a*, 1966*b*, 1966*c*), the growth rate for the radiated electromagnetic waves in both modes in the stream-plasma system is evaluated for some typical cases in the

* This equation gives the power radiated in both modes by a single electron in a magnetoactive plasma, and is discussed in more detail in Section III(*b*).

source region as observed from experiments. Subsequently, the propagation conditions (the escape conditions through the corona) for both modes are investigated; this includes the study of reflection levels and the first three harmonic resonance absorption levels. At the end of Section III we list the important predictions from the cyclotron theory and these are seen to agree closely with the observations. In Section IV, with the outcome of the theory developed, we conclude the interpretation of the solar type I phenomenon.

II. MODEL OF THE SOLAR CORONA

In order to investigate a plausible generating mechanism and the subsequent propagation conditions in a quantitative way, we need some models for the electron density distribution and spot-field configurations in the corona. In the possible source region, the Sun's general magnetic field, being very much smaller than the sunspot field, will be neglected in our consideration.

(a) *Electron Density Distribution Models in the Corona*

In the normal background corona, we will adopt the conventional Baumbach-Allen model (Allen 1947) for the radial distribution of electron density N , namely,

$$N = 10^8(1.55 \rho^{-6} + 2.99 \rho^{-16}) \quad \text{cm}^{-3}, \quad (2.1)$$

where $\rho = R/R_0$ and R is the distance from the centre of the Sun.

Corresponding to the electron density N , the electron plasma frequency f_p is given by $f_p = (Ne^2/\pi m_0)^{1/2}$, where e and m_0 are the electronic charge and rest mass of an electron respectively.

Optical and radio observations on electron density in the active coronal regions indicate that the electron density is around 5–10 times that given by relation (2.1) (Newkirk 1959; Shain and Higgins 1959; Morimoto and Kai 1962; Weiss 1963). We will therefore employ an electron density model which is $5 \times$ Baumbach-Allen or $10 \times$ Baumbach-Allen for the active regions in the corona.

(b) *Models of Spot-field Configurations*

Up to the present, there is no experimental result giving the magnitude and the exact nature of spot magnetic fields above the photosphere. However, we need some models for the spot-field configurations in order to investigate the theory quantitatively. We will specify below a model for a bipolar sunspot group and a model for a unipolar spot for this purpose. For more detailed discussions of sunspots, the reader is referred to Bray and Loughhead (1962, 1964).

Referring to Figure 1, we assume an imaginary dipole to be situated at a point P, at a distance PE below the photosphere. Some lines of force originating from this dipole emerge from a circular area a (spot area) on the Sun's surface. By choosing a suitable orientation of the imaginary dipole with respect to the radius of the Sun and the distance PE, one can obtain a situation where the field intensity at the point C, which is the centre of the spot, is the strongest in comparison to the intensity at any other point on a . It should be remarked that for a fixed value of the angle β

we can vary the distance PE in order to achieve this condition. With PR perpendicular to the axis of the dipole, angle $l' = L$ will be the latitude angle for the field line at the point C (l' = latitude angle with respect to PR). If, considering a particular field line, $r = r_0 \cos^2 l'$, where r is the radius vector at a point of the field line and r_0 is the distance between the middle point of the dipole axis and the point of minimum field strength along the line, the dipole field equation gives

$$H = Mr^{-3}(1 + 3 \sin^2 l')^{\frac{1}{2}}, \tag{2.2}$$

where M is a constant depending on the pole strength of the dipole.

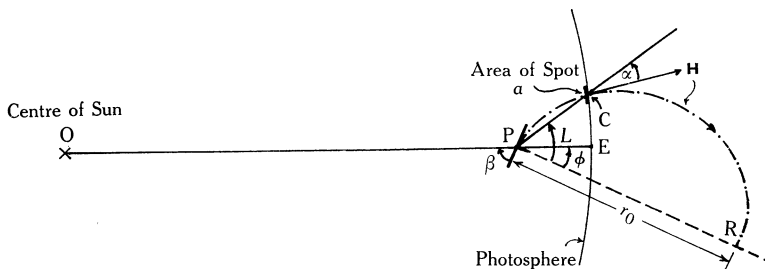


Fig. 1.—Geometry showing the calculation of a theoretical bipolar spot-field configuration. O is the centre of the Sun and P is the midpoint of the imaginary dipole. The arrow **H** represents the field line passing through the centre C of the leading spot of area a . PR is perpendicular to the axis of the dipole.

If we now let $PE = 0.1 R_0$, $\beta = 70^\circ$, $L = 60^\circ$, and $\phi = 20^\circ$ in our present case, and we let the field intensity at C be 2500 G, we find that the field strength of the field line passing through C is specified by

$$H = 8.4 r^{-3}(1 + 3 \sin^2 l')^{\frac{1}{2}} \tag{2.3}$$

and that $r = 0.63 \cos^2 l'$.

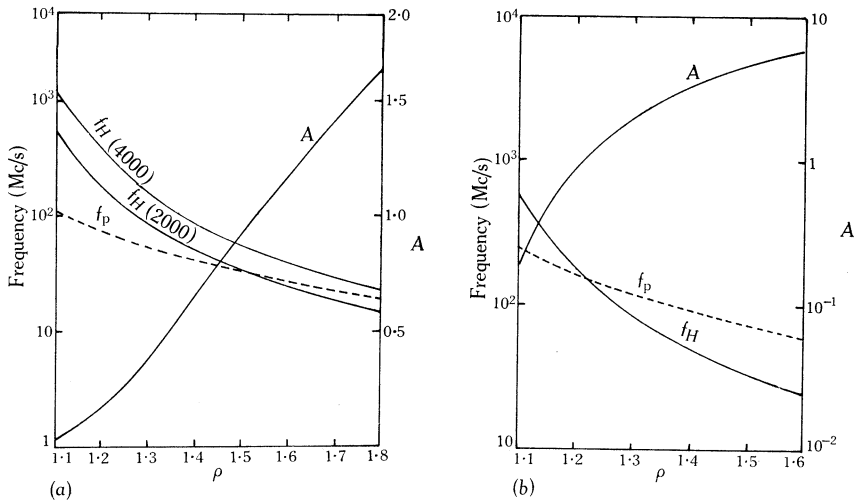
The field direction at any point along the field line is given by

$$\tan \alpha = \frac{1}{2} \cot l', \tag{2.4}$$

where α is the angle between the field line and the radius vector passing through the point in question.

Following the same method one can calculate the field intensity (equation similar to (2.3)) and the direction of the field vector **H** of any point along any of the field lines emerging from the spot area a . These field lines will terminate on the other spot of the associated sunspot pair. We note here that, although the field intensity at the centre of the spot on the photosphere is a maximum, the field line passing through this point may not be the strongest field line emerging through the spot. A very similar magnetic field model to the one described above was introduced by Takakura (1961).

When we consider a unipolar spot, we will assume that the axis of the imaginary dipole is along a radius vector of the Sun and only some lines of force from the pole nearer to the photosphere will emerge through an area (spot area) on the surface.



Figs. 2(a) and 2(b).—Variation of the plasma frequency f_p (using the Baumbach–Allen model (a) and the $5 \times$ Baumbach–Allen model (b)), gyrofrequency f_H , and $A (= f_p^2/f_H^2)$ along the strongest field line of a unipolar spot specified by $H_s = 2000$ G. The variation of f_H with ρ when $H_s = 4000$ G is also plotted in (a) for comparison.

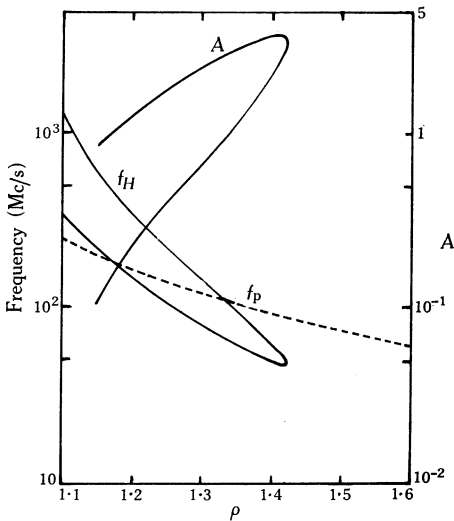


Fig. 2(c).—Variation of the plasma frequency f_p (using the $5 \times$ Baumbach–Allen model), gyrofrequency f_H , and A along the strongest field line of a bipolar spot group specified by $H_s = 2500$ G.

These field lines are supposed to be straight, extending to the corona, and the line passing through the centre of the spot will be the strongest field line, with magnetic intensity at a height $(\rho-1)$ being specified by (Ginzburg 1964, p. 413)

$$H = H_s[1 - (\rho - 1) / \{(\rho - 1)^2 + b^2\}^{1/2}], \tag{2.5}$$

where b is the radius of the sunspot in units of solar radii and H_s is the maximum field intensity of the spot. Following Ginzburg, we take b to be 0.05.

Some examples of theoretical spot-field configurations and electron density distributions are indicated in Figure 2.

III. CYCLOTRON RADIATION FROM ELECTRON STREAMS GYRATING IN SPOT-FIELD CONFIGURATIONS

(a) *Emitted Frequency Range from Electrons*

We will, first of all, assume the existence of electrons spiralling along spot magnetic field lines in the source region. When the spot-field configuration is bipolar in nature, electrons gyrating along a particular field line will be mirrored and trapped for some time before diffusing away. It is well known that each electron will radiate a range of frequencies at any instant. If the electron acquires a kinetic energy of the order of 1 MeV, synchrotron radiation results and the bandwidth of emission will be very wide, which is not observed. We therefore assume that the energy of the radiating electron is of the order of 10–100 keV (cyclotron radiation will be emitted for this order of energy), and we will discuss the possible range of frequencies radiated from such electrons.

In considering the cyclotron process, we will assume that the collisionless Appleton–Hartree equation is valid in the solar corona, based on the fact that the mean thermal velocity β_T of electrons in the background corona is small, being $\sim 10^{-2}$ (Ginzburg 1964, p. 121). The refractive index n_j for an electromagnetic wave in the background corona alone is given by

$$n_j^2 = 1 - \frac{A\xi^{-2}(1-A\xi^{-2})}{1-A\xi^{-2} - \frac{1}{2}\xi^{-2}\sin^2\theta \mp \{\frac{1}{4}\xi^{-4}\sin^4\theta + (1-A\xi^{-2})^2\xi^{-2}\cos^2\theta\}^{\frac{1}{2}}}, \quad (3.1)$$

where $A = \omega_p^2/\omega_H^2$ is a quantity specifying the magnetoactive plasma, $\omega_p = 2\pi f_p$, $\omega_H = 2\pi f_H$, $f_p^2 = Ne^2/\pi m$, $f_H = |e|H_0/2\pi m_0 c$, H_0 is the static magnetic intensity due to the spot field, θ , the wave-normal angle, is the angle between the wave vector \mathbf{k} and the vector \mathbf{H}_0 , $\xi = f/f_H$, $f (= \omega/2\pi)$ is the wave frequency, and c is the speed of light in a vacuum.

Since the majority of noise storms are observed to occur at altitudes between about 0.2 and 0.5 R_0 , and a typical value of the maximum field intensity in the spot area is $H_s = 2000$ G for a noise storm to occur, we can set up limits for the quantity A in the possible source region. Here, of course, we have to assume that in most cases the apparent source positions are the real source positions. Within the regime of the above assumptions, A is found to range from about 0.2 to 5. To show a typical example of the form of equation (3.1), in Figure 3 the refractive index n_j is plotted as a function of the normalized frequency $\xi = f/f_H$ for the wave-normal angle $\theta = 10^\circ$ and 75° in the case where $A = 1$. The curves marked o and x are refractive index curves for the o- and x-modes respectively.

It is easy to show from the refractive index expression that for all values of θ in the x-mode, when $n_j = 0$, ξ is given by

$$\xi_x = \frac{1}{2}\{1 + (1 + 4A)\}^{\frac{1}{2}} > 1. \quad (3.2)$$

In the o-mode, for all values of θ not equal to 0° , $\xi = \xi_0$ when $n_j = 0$, and

$$\xi_0 = A^{\frac{1}{2}}. \quad (3.3)$$

For an observer in a reference system fixed to the background magnetoactive plasma in which an electron is gyrating, the observed radiated frequency is given by the Doppler equation

$$\xi = s\gamma/(1 - n_j \beta_{\parallel} \cos \theta), \quad (3.4)$$

where n_j must satisfy (3.1). In equation (3.4) $\gamma = (1 - \beta_{\perp}^2 - \beta_{\parallel}^2)^{-1/2}$, $\beta_{\perp} = v_{\perp}/c$ is the normalized transverse velocity, $\beta_{\parallel} = v_{\parallel}/c$ is the normalized longitudinal velocity, v_{\perp} and v_{\parallel} are the velocities of the electron in directions perpendicular and parallel to the static magnetic field direction respectively, and s is the harmonic number.

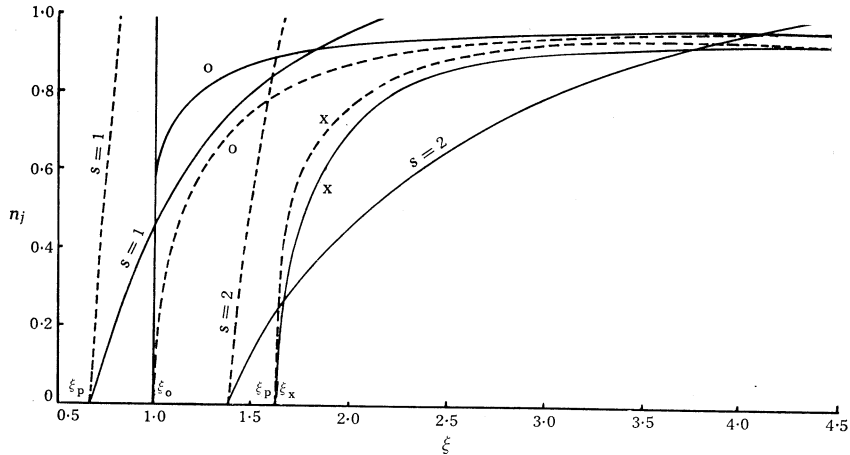


Fig. 3.—Refractive index n_j for the o-mode and x-mode against normalized wave frequency ξ for $A = 1$, and $\theta = 10^\circ$ (full lines) and 75° (dashed lines). The Doppler equation is also plotted for the first two harmonics, $s = 1$, $s = 2$, as a function of ξ for $\beta_{\perp} = 0.3$, $\beta_{\parallel} = 0.7$.

The frequency corresponding to $n_j = 0$ is independent of θ and is given by

$$\xi_D = s\gamma. \quad (3.5)$$

In Figure 3 the Doppler equation is plotted for the first two harmonics ($s = 1, 2$), taking $\theta = 10^\circ$ and 75° and $\beta_{\perp} = 0.3$, $\beta_{\parallel} = 0.7$.

It is clear from Figure 3 that there can be one or two simultaneous solutions (i.e. points of intersection) of the dispersion and Doppler equations depending on whether

$$\xi_D = s\gamma \geq \xi_{o,x} \quad (3.6a)$$

or

$$s\gamma < \xi_{o,x}. \quad (3.6b)$$

We refer to these two cases as the “single” (3.6a) and “double” (3.6b) frequency solutions respectively. These two different solutions show up clearly in Figure 4, where simultaneous solutions of equations (3.1) and (3.4) are plotted for the o-mode (Fig. 4(a)) and the x-mode (Fig. 4(b)). The double solutions have a limited θ range. We denote the upper limit by the cut-off angle θ_c , which corresponds to the Doppler equation being a tangent to the dispersion equation. These two types of solutions for the normalized frequency ξ are very important in the explanation of bursts and

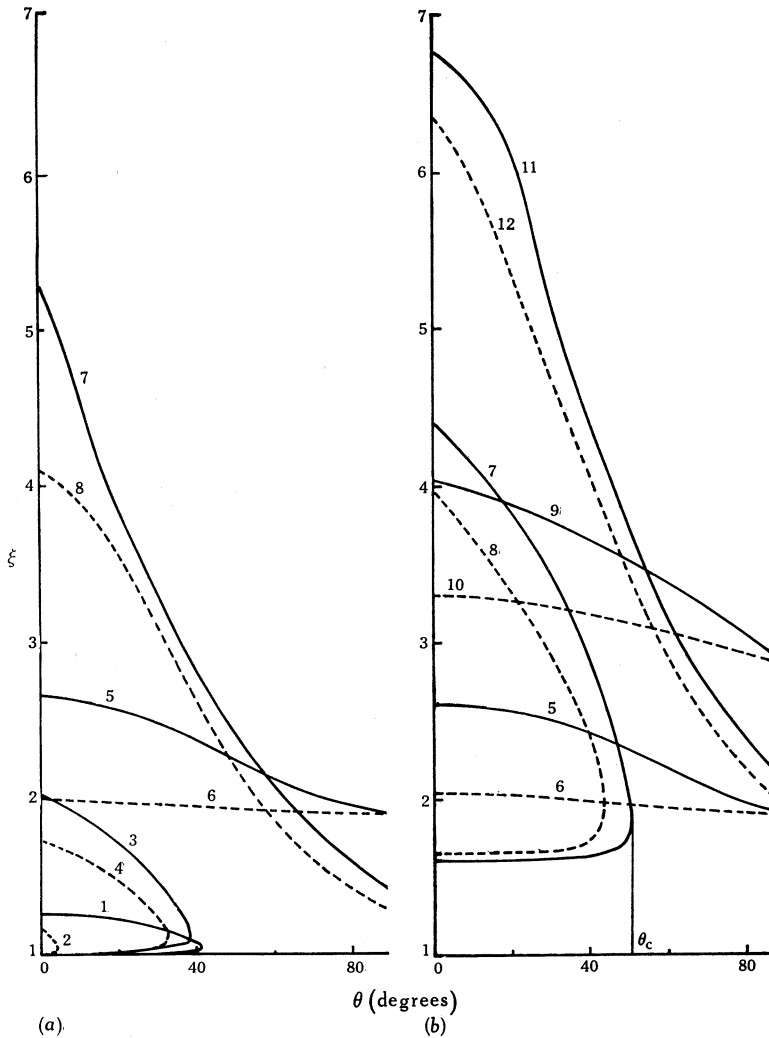


Fig. 4.—Relation between normalized frequency ξ and wave-normal angle θ for $A = 1$ for (a) o-mode and (b) x-mode waves. Values of other parameters for the curves are:

- | | |
|---|---|
| 1, $s = 1, \beta_{\perp} = 0.1, \beta_{\parallel} = 0.3$; | 2, $s = 1, \beta_{\perp} = 0.3, \beta_{\parallel} = 0.1$; |
| 3, $s = 1, \beta_{\perp} = 0.1, \beta_{\parallel} = 0.7$; | 4, $s = 1, \beta_{\perp} = 0.3, \beta_{\parallel} = 0.7$; |
| 5, $s = 2, \beta_{\perp} = 0.1, \beta_{\parallel} = 0.3$; | 6, $s = 2, \beta_{\perp} = 0.3, \beta_{\parallel} = 0.1$; |
| 7, $s = 2, \beta_{\perp} = 0.1, \beta_{\parallel} = 0.7$; | 8, $s = 2, \beta_{\perp} = 0.3, \beta_{\parallel} = 0.7$; |
| 9, $s = 3, \beta_{\perp} = 0.1, \beta_{\parallel} = 0.3$; | 10, $s = 3, \beta_{\perp} = 0.3, \beta_{\parallel} = 0.1$; |
| 11, $s = 3, \beta_{\perp} = 0.1, \beta_{\parallel} = 0.7$; | 12, $s = 3, \beta_{\perp} = 0.3, \beta_{\parallel} = 0.7$. |

continuum radiation and should always be kept in mind. It should be noted that, for given β_{\perp} and β_{\parallel} , a *double* solution for the x-mode usually occurs at a harmonic number that is one unit larger than that for the *double* solution of the o-mode.

(b) Power Spectrum of a Single Electron

An electron emits cyclotron radiation in both ordinary and extraordinary modes. It is necessary to investigate whether only one of the two modes or both carry significant energy and are capable of escaping through the corona. With various values of β_{\perp} and β_{\parallel} for the radiating electron, the emitted normalized frequency ξ has been obtained as a function of the wave-normal angle θ for the three values of A of 0.25, 1, and 1.5 (we have shown an example of the graph for $A = 1$ only). Eidman (1958, 1959) gives the expression for the electromagnetic power radiated in both modes by a single electron in a magnetoactive plasma. The equation was later re-derived by Liemohn (1965), who corrected a few errors in Eidman's work. Using the corrected Eidman equation, we now evaluate the power spectra emitted by single electrons in the two modes with parameters corresponding to those in Section (a). For an electron gyrating with pitch angle $\phi = \text{artan}(\beta_{\perp}/\beta_{\parallel})$ and with the guiding centre along the z direction, the power radiated at θ per unit solid angle in the s th harmonic is

$$P_s = \left(\frac{e^2}{2\pi c}\right) \left(\frac{\omega^2 n_j K^2 \{-\beta_{\perp} J'_s(a) + (\alpha_y s \beta_{\perp}/a + \alpha_z \beta_{\parallel}) J_s(a)\}^2 \{1 + (\omega/n_j) \partial n_j / \partial \omega\}}{|1 - \beta_{\parallel} n_j \{1 + (\omega/n_j) \partial n_j / \partial \omega\} \cos \theta|}\right), \quad (3.7a)$$

where

$$\alpha_y = \alpha_{\theta} \cos \theta + \alpha_K \sin \theta, \quad \alpha_z = \alpha_K \cos \theta - \alpha_{\theta} \sin \theta,$$

$$K = (1 + \alpha_{\theta}^2)^{-\frac{1}{2}},$$

$$\alpha_{\theta} = -\xi \cos \theta / \{\xi^2 + A/(n_j^2 - 1)\}, \quad \alpha_K = -\xi(n_j^2 - 1) \sin \theta / (A - \xi^2),$$

and J_s and J'_s are Bessel's function and its derivative with argument $a = n_j \beta_{\perp} \xi \sin \theta / \gamma$. We have also

$$\frac{\omega}{n_j} \frac{\partial n_j}{\partial \omega} = \frac{A}{2n_j^2 \xi^2 D^2} \left(2(1 - 2A\xi^{-2})D + (1 - A\xi^{-2})(2A\xi^{-2} + \xi^{-2} \sin^2 \theta \pm \frac{1}{2} B^{-\frac{1}{2}} E)\right), \quad (3.7b)$$

where

$$D = 1 - A\xi^{-2} - \frac{1}{2}\xi^{-2} \sin^2 \theta - B^{\frac{1}{2}},$$

$$E = -\xi^{-4} \sin^4 \theta - 2\xi^{-2} \cos^2 \theta (1 - 2A\xi^{-2})(1 - 3A\xi^{-2}),$$

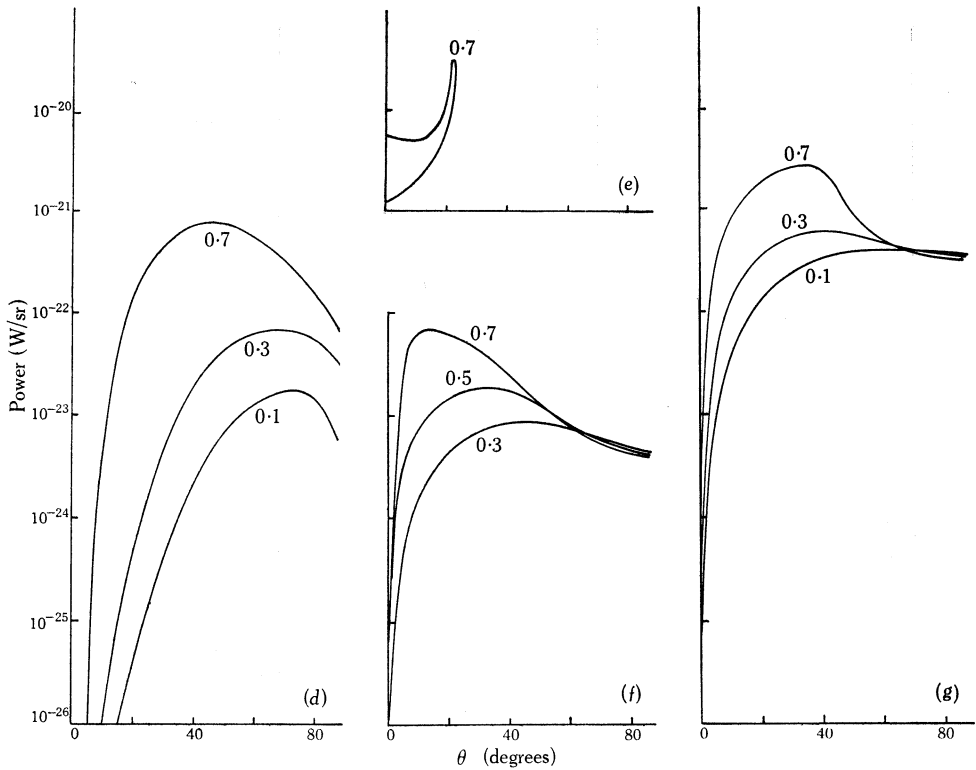
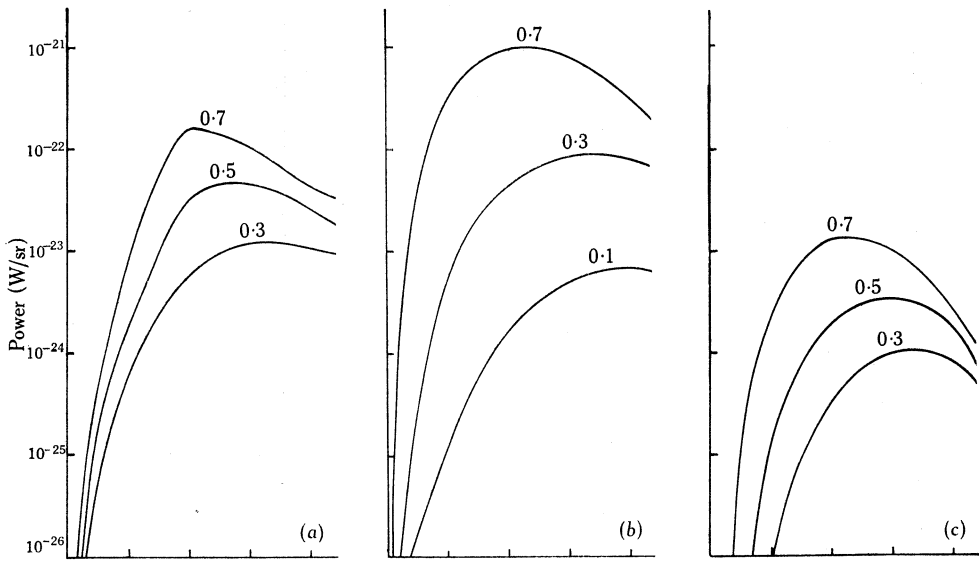
$$B = \frac{1}{4}\xi^{-4} \sin^4 \theta + \xi^{-2} \cos^2 \theta (1 - A\xi^{-2})^2,$$

and the positive and negative signs of the last term in (3.7b) correspond to the o-mode and the x-mode respectively.

The result of the computations for the two lowest possible harmonics ($s = 1, 2$ or $2, 3$) in both the o- and x-modes for various values of electron energy and pitch

Figs. 5(a) to 5(g).—Power spectrum radiated by a single electron for $A = 0.25, f_H = 100$ Mc/s,

- (a) o-mode, $s = 1, \beta_{\perp} = 0.1, \beta_{\parallel} = 0.3, 0.5, 0.7$;
- (b) o-mode, $s = 1, \beta_{\perp} = 0.3, \beta_{\parallel} = 0.1, 0.3, 0.7$;
- (c) o-mode, $s = 2, \beta_{\perp} = 0.1, \beta_{\parallel} = 0.3, 0.5, 0.7$;
- (d) o-mode, $s = 2, \beta_{\perp} = 0.3, \beta_{\parallel} = 0.1, 0.3, 0.7$;
- (e) x-mode, $s = 1, \beta_{\perp} = 0.1, \beta_{\parallel} = 0.7$;
- (f) x-mode, $s = 2, \beta_{\perp} = 0.1, \beta_{\parallel} = 0.3, 0.5, 0.7$;
- (g) x-mode, $s = 2, \beta_{\perp} = 0.3, \beta_{\parallel} = 0.1, 0.3, 0.7$.



Figs. 5(a) to 5(g)

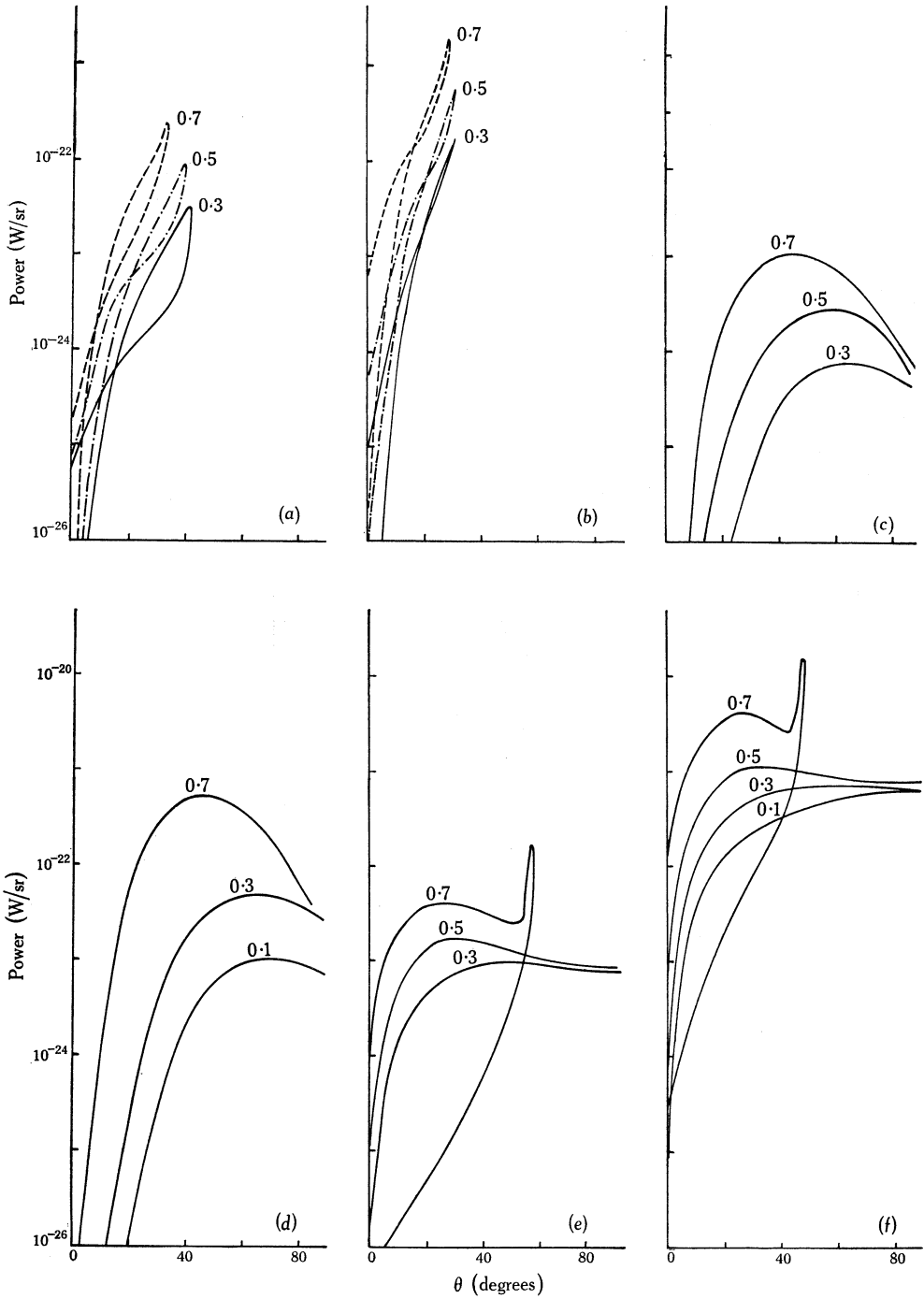
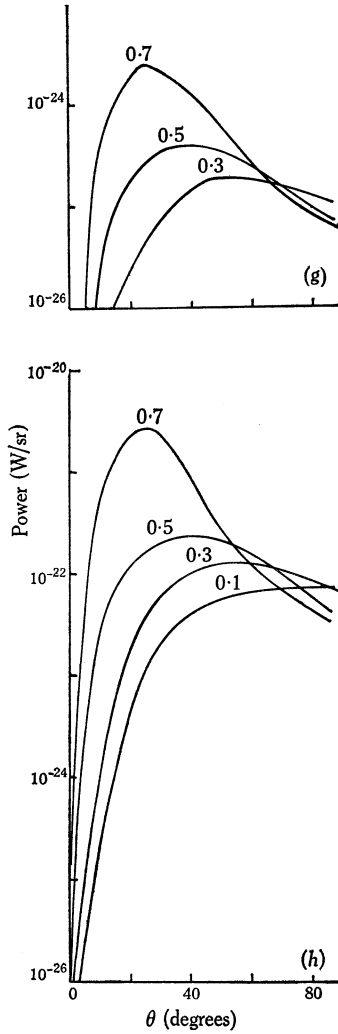


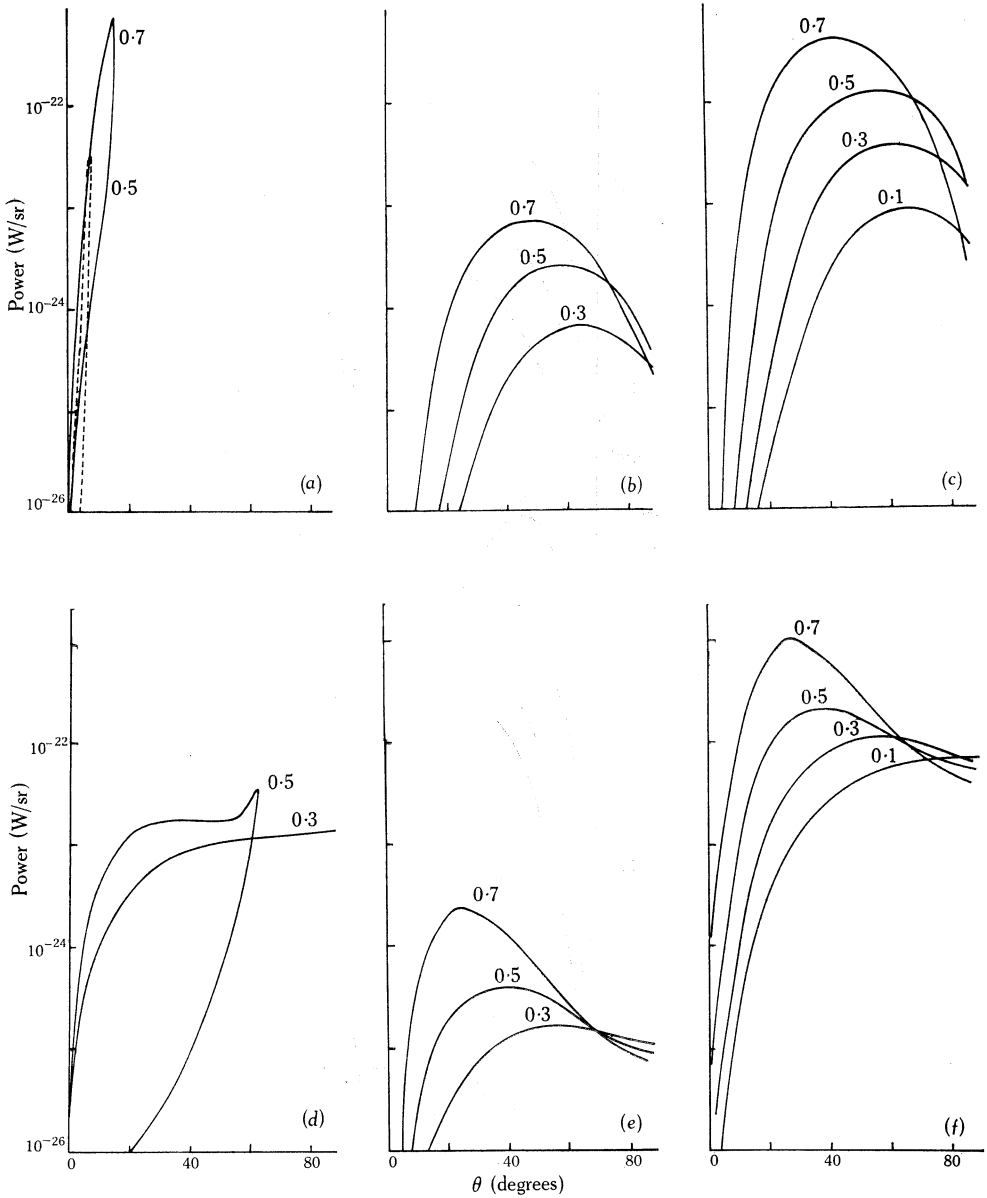
Fig. 6 (continued on facing page)

Fig. 6 (Continued)



Figs. 6(a) to 6(h).—Power spectrum radiated by a single electron for $A = 1$, $f_H = 100$ Mc/s, and

- (a) o-mode, $s = 1$, $\beta_{\perp} = 0.1$, $\beta_{\parallel} = 0.3, 0.5, 0.7$;
- (b) o-mode, $s = 1$, $\beta_{\perp} = 0.3$, $\beta_{\parallel} = 0.3, 0.5, 0.7$;
- (c) o-mode, $s = 2$, $\beta_{\perp} = 0.1$, $\beta_{\parallel} = 0.3, 0.5, 0.7$;
- (d) o-mode, $s = 2$, $\beta_{\perp} = 0.3$, $\beta_{\parallel} = 0.1, 0.3, 0.7$;
- (e) x-mode, $s = 2$, $\beta_{\perp} = 0.1$, $\beta_{\parallel} = 0.3, 0.5, 0.7$;
- (f) x-mode, $s = 2$, $\beta_{\perp} = 0.3$, $\beta_{\parallel} = 0.1, 0.3, 0.5, 0.7$;
- (g) x-mode, $s = 3$, $\beta_{\perp} = 0.1$, $\beta_{\parallel} = 0.3, 0.5, 0.7$;
- (h) x-mode, $s = 3$, $\beta_{\perp} = 0.3$, $\beta_{\parallel} = 0.1, 0.3, 0.5, 0.7$.



Figs. 7(a) to 7(f).—Power spectrum radiated by a single electron for $A = 1.5$, $f_H = 100$ Mc/s, and

- (a) o-mode, $s = 1$, $\beta_{\perp} = 0.1$, $\beta_{\parallel} = 0.5, 0.7$;
- (b) o-mode, $s = 2$, $\beta_{\perp} = 0.1$, $\beta_{\parallel} = 0.3, 0.5, 0.7$;
- (c) o-mode, $s = 2$, $\beta_{\perp} = 0.3$, $\beta_{\parallel} = 0.1, 0.3, 0.5, 0.7$;
- (d) x-mode, $s = 2$, $\beta_{\perp} = 0.1$, $\beta_{\parallel} = 0.3, 0.5$;
- (e) x-mode, $s = 3$, $\beta_{\perp} = 0.1$, $\beta_{\parallel} = 0.3, 0.5, 0.7$;
- (f) x-mode, $s = 3$, $\beta_{\perp} = 0.3$, $\beta_{\parallel} = 0.1, 0.3, 0.5, 0.7$.

angle (specified by $\beta_{\perp} = 0.1, \beta_{\parallel} = 0.3, 0.5, 0.7$ and $\beta_{\perp} = 0.3, \beta_{\parallel} = 0.1, 0.3, 0.5, 0.7$) and for different background plasmas specified by different values of A are presented in Figures 5 ($A = 0.25$), 6 ($A = 1$), and 7 ($A = 1.5$). From these diagrams, we note that for such ranges of energy and pitch angle of the radiator we have the following properties:

- (1) For the *single* frequency solution, the power of the x-mode maximizes at θ ranging from 15° to 45° , while an o-mode wave carries most power at θ ranging from 40° to 70° .
- (2) For the *double* frequency solution, energy of the wave maximizes at a direction very close to the cut-off angle θ_c for both the o- and x-modes. Much more power is radiated by an electron whenever the *double* frequency solution exists.
- (3) When $\beta_{\perp}, \beta_{\parallel}$, and the harmonic number s are kept constant, the maximum power carried by the x-mode wave exceeds that of the o-mode wave by about one to two orders of magnitude.
- (4) With increasing harmonic number, the radiated power decreases with increasing value of s .
- (5) As it has been mentioned, in order to have the *double* frequency solution the harmonic number for the x-mode wave will usually be one unit larger than that for the o-mode wave, and hence from points (3) and (4) we observe that the power radiated by both characteristic modes can be of the same order of magnitude for the cases of a *double* frequency solution.

(c) *Amplification of Electromagnetic Waves in a Stream-Plasma System*

So far, we have considered radiation spectra from single electrons only. It has been pointed out correctly by Ginzburg and Zheleznyakov (1961) that incoherent cyclotron radiation from electrons cannot account for the high flux density of storm bursts received on the Earth. We will assume here that electron streams exist in the active solar corona and that some are trapped in the sunspot magnetic fields. If the energetic electrons come from explosions or dumping from plasma clouds, those electrons travelling at almost the same velocity and pitch angle will form a stream having a small spread in momentum distribution. In another terminology, we say that such an electron stream has a finite temperature that is a measure of the momentum spread. Since the bandwidth of a type I burst is very narrow ($\Delta f/f \sim 0.04$), the spread in momentum distribution of the radiating stream must be very small for many circumstances. The instability problem of such a stream-plasma system (when the temperature effect is taken into account) has been solved by Fung (1966c). On account of the complexity in the mathematics for such a system, we will assume here that the temperature of the electron stream is zero, i.e. every electron in the stream has the same values of $p_{\perp} = p_{\perp}^0$ and $p_{\parallel} = p_{\parallel}^0$ and the stream is called "helical". This helical-stream-plasma instability theory has been applied to the terrestrial v.l.f. case and to the case of decametric radiation from Jupiter (Fung 1966a, 1966b). Even though a helical stream is the limiting case of a realistic one, the instability theory gives the same general behaviour of the growth rate as in the case when

temperature is included.* We will therefore, without loss of generality in the outcome of the result, assume that the stream is helical, and the distribution function of the stream will be given by

$$f_0(\vec{p}) d\vec{p} = (1/2\pi p_{\perp}^0) \delta(p_{\perp} - p_{\perp}^0) \delta(p_{\parallel} - p_{\parallel}^0) d\vec{p}, \quad (3.8)$$

where p_{\perp} , p_{\parallel} are transverse and longitudinal momenta respectively and δ is the Dirac delta.

In considering the growth of a wave in the course of time, we assume the vector k to be real and write the complex angular frequency as

$$\omega = \tilde{\omega} + \delta,$$

where $\tilde{\omega}$, being real, is called the "characteristic frequency"; it is the frequency radiated by a single particle alone in the magnetoactive plasma. The imaginary part of ω gives the growth rate and the growth factor will be $\exp(\text{Im } \delta)t$. Assuming the particle density of the stream to be small compared with that of the ambient plasma, the growth rate of an electromagnetic wave in the stream-plasma system is given by Fung (1966*b*) as

$$\text{Im}(\delta/\tilde{\omega}) = \pm(\frac{1}{2}\sqrt{3})(M^{\frac{1}{2}} - C^{\frac{1}{2}}), \quad (3.9)$$

where

$$M = -\frac{1}{2}d + (\frac{1}{4}d^2 + b^3/27)^{\frac{1}{2}} \quad \text{and} \quad C = -\frac{1}{2}d - (\frac{1}{4}d^2 - b^3/27)^{\frac{1}{2}},$$

$$\text{with} \quad b = -\sigma A J_s^2 \left(\frac{(s\gamma - \xi)^2}{\beta_{\parallel}^2 \xi^2} - 1 \right) \frac{\beta_{\parallel}^2 \cos^2 \theta}{(\xi - s\gamma)^2},$$

$$d = \sigma A \left(\frac{(s\gamma - \xi)^2}{\beta_{\parallel}^2 \xi^2} - 1 \right) \frac{J_s^2 \beta_{\perp}^2 + J_s^2 \beta_{\parallel}^2 (s\gamma - \xi \sin^2 \theta)^2 / (s\gamma - \xi)^2 \sin^2 \theta}{(AL - 2\xi^2)},$$

$$L = \frac{1}{D^2} \left[\frac{2AD}{\xi^2} - \left(1 - \frac{A}{\xi^2} \right) \left(\frac{2A}{\xi^2} + \frac{\sin^2 \theta}{\xi^2} - B^{\frac{1}{2}} \left[-\frac{\sin^4 \theta}{\xi^4} + \frac{4A \cos^2 \theta}{\xi^4} \left(1 - \frac{A}{\xi^2} \right) - \frac{2 \cos^2 \theta}{\xi^2} \left(1 - \frac{A}{\xi^2} \right)^2 \right] \right] \right].$$

In expression (3.9) for small σ we have

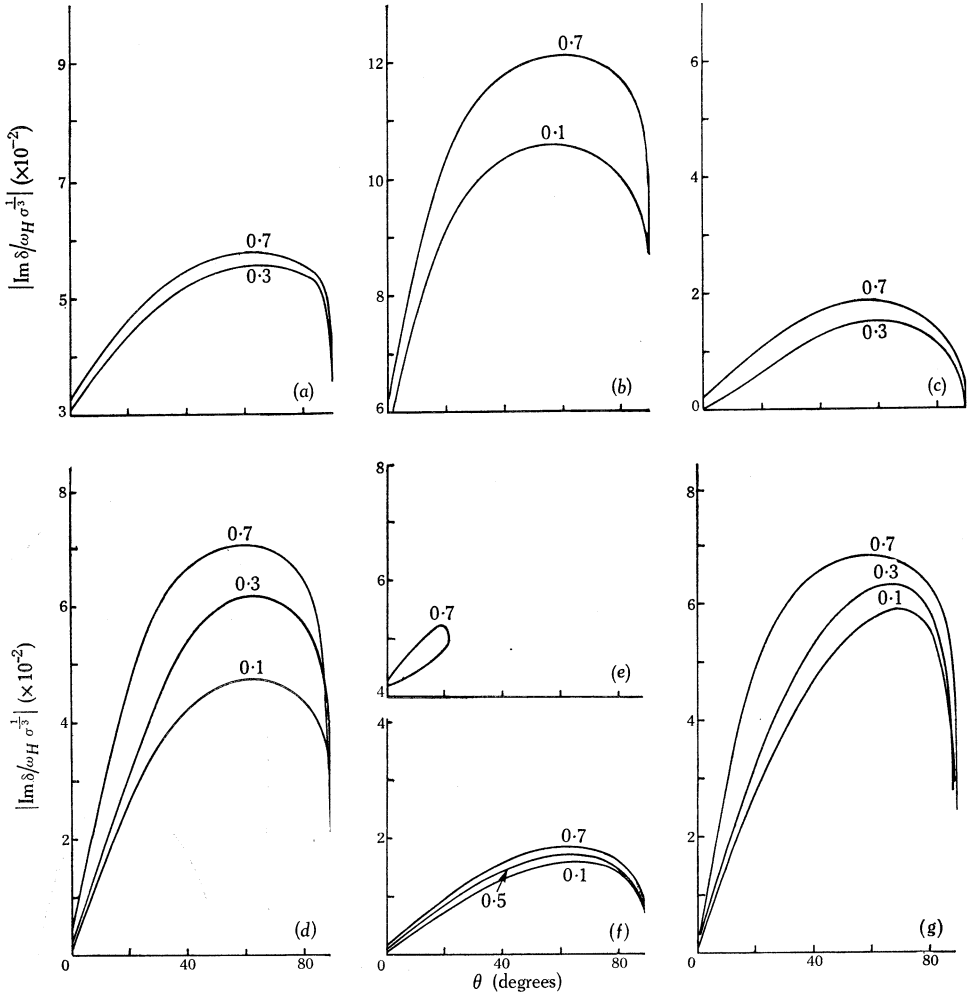
$$\frac{1}{4}d^2 \gg |b^3|/27, \quad (3.10)$$

and we can specify the growth rate in the following form

$$|\text{Im } \delta/\omega_H \sigma^{\frac{1}{2}}| = (\frac{1}{2}\sqrt{3})\xi(|d/\sigma|)^{\frac{1}{2}}. \quad (3.11)$$

Fixing the energy and pitch angle of the helical stream, the emitted characteristic normalized frequency ξ has been obtained as a function of the wave-normal angle θ for three values of A , 0.25, 1, and 1.5. The dependence of the growth rate (specified by $|\text{Im } \delta/\omega_H \sigma^{\frac{1}{2}}|$) on the wave-normal angle θ for both modes is shown in

* This statement is true only when the temperature of the stream is low; when the momentum spread is wide, the bandwidth of emission will be broad and the harmonics may not be resolved.

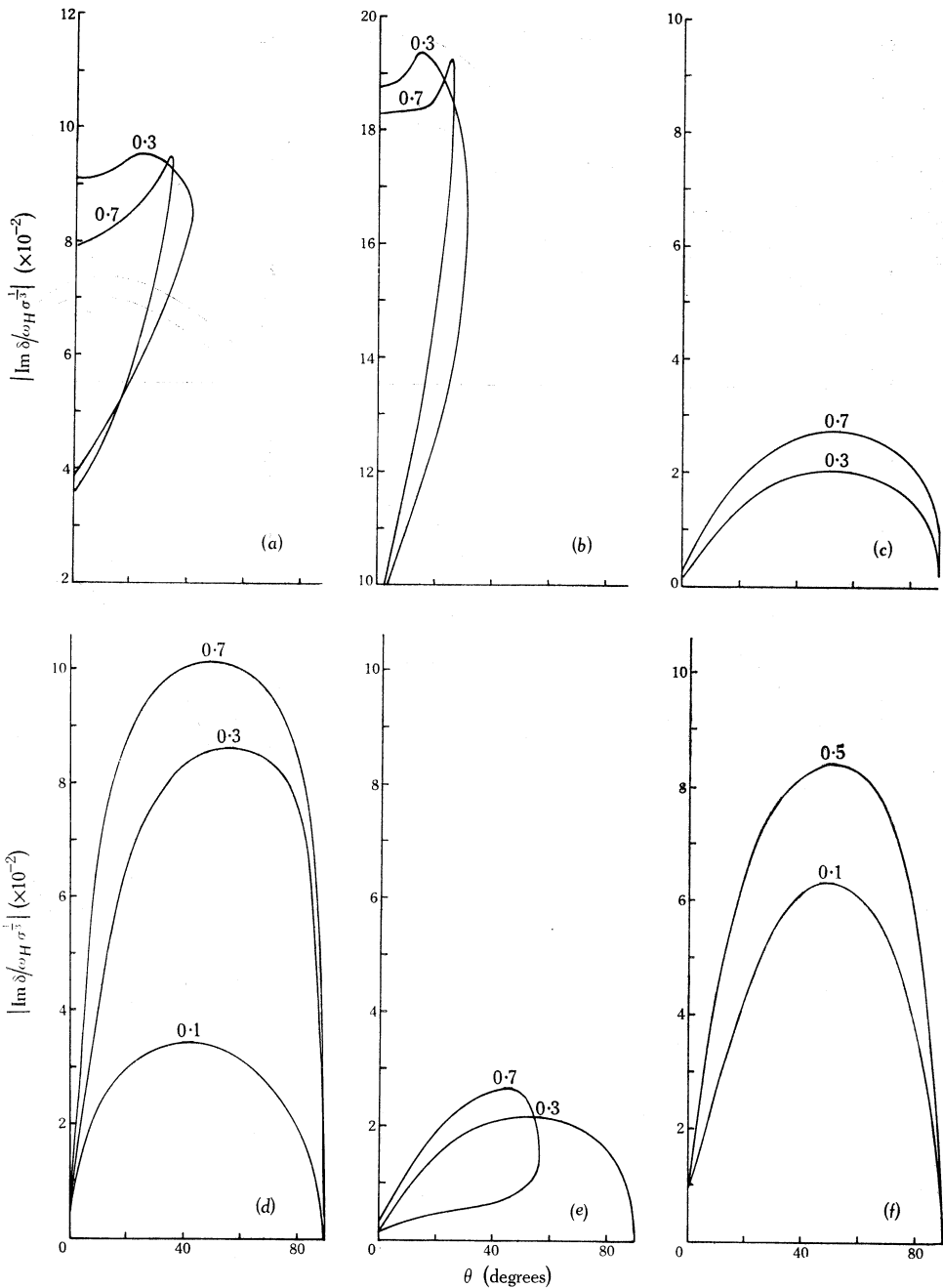


Figs. 8(a) to 8(g).—The dependence of the growth rate $|\text{Im } \delta/\omega_H \sigma^s|$ on wave-normal angle θ for $A = 0.25$ and

- (a) o-mode, $s = 1$, $\beta_{\perp} = 0.1$, $\beta_{\parallel} = 0.3, 0.7$;
- (b) o-mode, $s = 1$, $\beta_{\perp} = 0.3$, $\beta_{\parallel} = 0.1, 0.7$;
- (c) o-mode, $s = 2$, $\beta_{\perp} = 0.1$, $\beta_{\parallel} = 0.3, 0.7$;
- (d) o-mode, $s = 2$, $\beta_{\perp} = 0.3$, $\beta_{\parallel} = 0.1, 0.3, 0.7$;
- (e) x-mode, $s = 1$, $\beta_{\perp} = 0.1$, $\beta_{\parallel} = 0.7$;
- (f) x-mode, $s = 2$, $\beta_{\perp} = 0.1$, $\beta_{\parallel} = 0.1, 0.5, 0.7$;
- (g) x-mode, $s = 2$, $\beta_{\perp} = 0.3$, $\beta_{\parallel} = 0.1, 0.3, 0.7$.

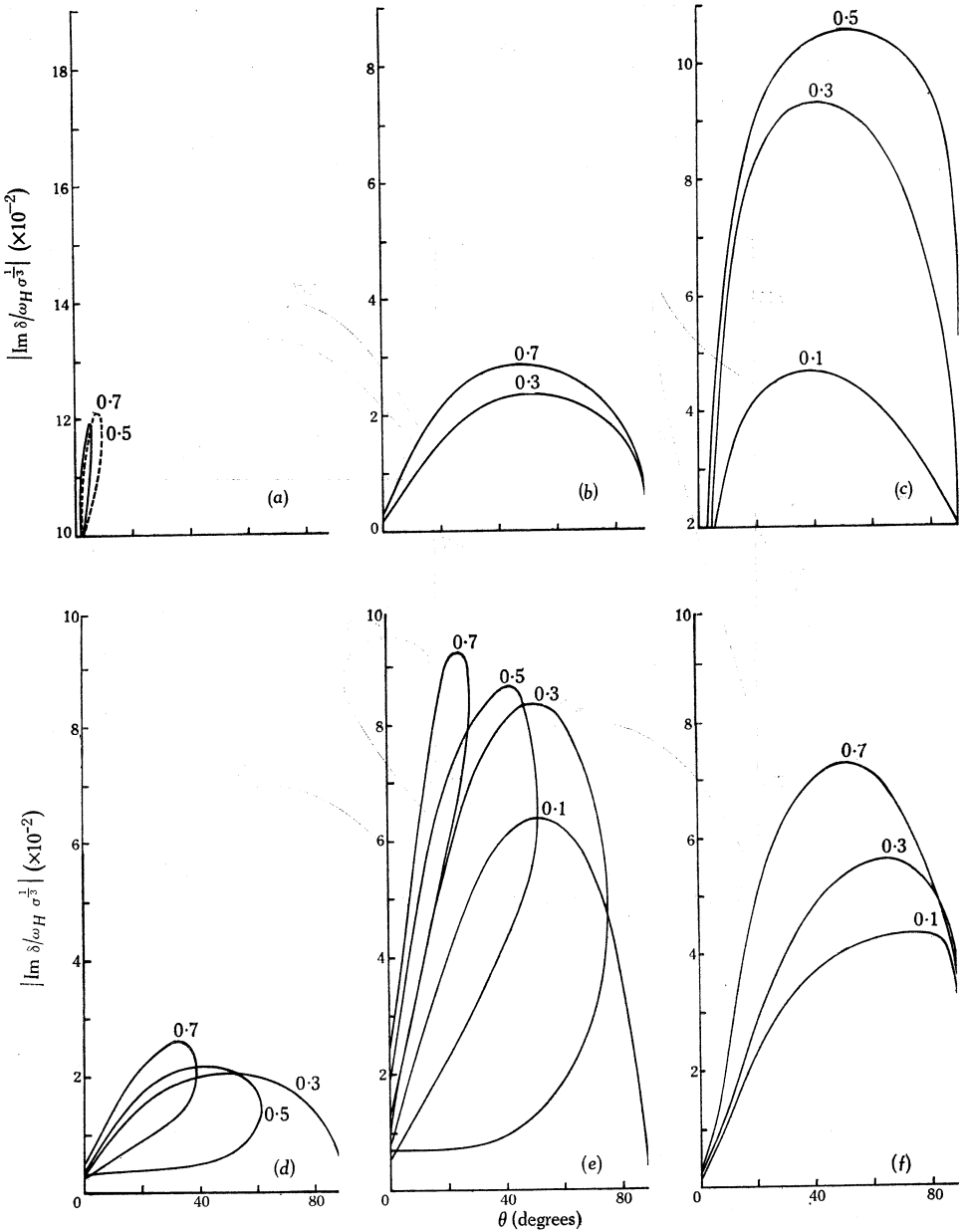
Figures 8–10 for frequencies and other parameters as in Figures 5–7. These graphs show the following features:

- (1) For the *single* frequency solution, the growth rate for the o-mode has a broad maximum around $\theta = \theta_m$ varying from 35° to 60° , while the growth rate for the x-mode also shows a broad maximum around θ_m , which ranges from 40° to 80° for various values of β_{\perp} , β_{\parallel} , and A as specified.



Figs. 9(a) to 9(f).—The dependence of the growth rate $|\text{Im } \delta/\omega_H \sigma^3|$ on wave-normal angle θ for $A = 1$ and

- (a) o-mode, $s = 1$, $\beta_{\perp} = 0.1$, $\beta_{\parallel} = 0.3, 0.7$; (b) o-mode, $s = 1$, $\beta_{\perp} = 0.3$, $\beta_{\parallel} = 0.3, 0.7$;
- (c) o-mode, $s = 2$, $\beta_{\perp} = 0.1$, $\beta_{\parallel} = 0.3, 0.7$; (d) o-mode, $s = 2$, $\beta_{\perp} = 0.3$, $\beta_{\parallel} = 0.1, 0.3, 0.7$;
- (e) x-mode, $s = 2$, $\beta_{\perp} = 0.1$, $\beta_{\parallel} = 0.3, 0.7$; (f) x-mode, $s = 2$, $\beta_{\perp} = 0.3$, $\beta_{\parallel} = 0.1, 0.5$.



Figs. 10(a) to 10(f).—The dependence of the growth rate $|\text{Im } \delta / \omega_H \sigma^3|$ on wave-normal angle θ for $A = 1.5$ and

- (a) o-mode, $s = 1$, $\beta_{\perp} = 0.1$, $\beta_{||} = 0.5, 0.7$;
- (b) o-mode, $s = 2$, $\beta_{\perp} = 0.1$, $\beta_{||} = 0.3, 0.7$;
- (c) o-mode, $s = 2$, $\beta_{\perp} = 0.3$, $\beta_{||} = 0.1, 0.3, 0.5$;
- (d) x-mode, $s = 2$, $\beta_{\perp} = 0.1$, $\beta_{||} = 0.3, 0.5, 0.7$;
- (e) x-mode, $s = 2$, $\beta_{\perp} = 0.3$, $\beta_{||} = 0.1, 0.3, 0.5, 0.7$;
- (f) x-mode, $s = 3$, $\beta_{\perp} = 0.3$, $\beta_{||} = 0.1, 0.3, 0.7$.

- (2) For both modes, whenever the *double* frequency solution exists, the growth rate is large and θ_m occurs near the cut-off angle θ_c . For a constant value of β_{\perp} , θ_m approaches θ_c as the pitch angle of the stream decreases (i.e. increasing β_{\parallel}). Moreover, when β_{\perp} is fixed, the value of maximum growth rate increases with increasing β_{\parallel} up to an optimum value of β_{\parallel} ; then the maximum growth decreases with still increasing β_{\parallel} .

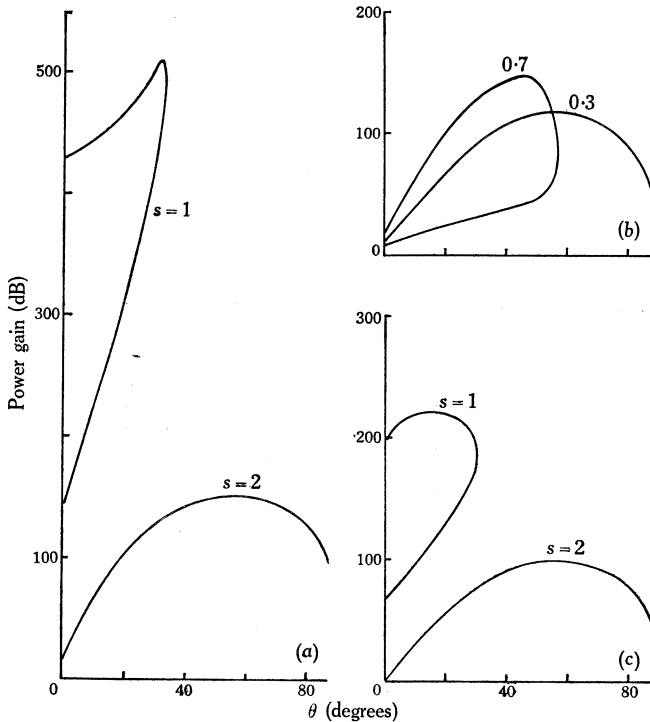


Fig. 11.—Power gain versus wave-normal angle θ for $f_H = 100$ Mc/s, $A = 1$, and
 (a) o-mode, $s = 1, 2$, $\beta_{\perp} = 0.1$, $\beta_{\parallel} = 0.7$, $\sigma = \omega_0^2/\omega_p^2 = 10^{-3}$, interaction time = 10^{-5} sec;
 (b) x-mode, $s = 2$, $\beta_{\perp} = 0.1$, $\beta_{\parallel} = 0.3, 0.7$, $\sigma = 10^{-3}$, interaction time = 10^{-5} sec;
 (c) o-mode, $s = 1, 2$, $\beta_{\perp} = 0.3$, $\beta_{\parallel} = 0.3$, $\sigma = 10^{-6}$, interaction time = 4×10^{-5} sec.

- (3) With the range of values for A as assigned (0.25–1.5), the growth rates for both modes in the same harmonic are of the same order of magnitude.
- (4) The growth rate decreases rapidly with increasing harmonic number for electron energy of the order of 10–100 keV. This means that the power radiated in the o-mode in the fundamental harmonic by a stream of electrons would by far exceed the power radiated in the x-mode in the second harmonic.

In this stream-plasma system, the electromagnetic wave grows exponentially as a function of time. If we assume that the wave interacts for 10^{-5} sec (or 4×10^{-5} sec) with the stream, that σ (the density of the stream)/(the density of

the ambient plasma) = 10^{-3} (or 10^{-6}), and that the gyrofrequency $f_H = \omega_H/2\pi = 100$ Mc/s, we can calculate the power gain after this short period of interaction. We show some examples of the relation between the power gain in decibels and the wave-normal angle θ in Figure 11. Corresponding relations between the power gain and the normalized frequency are given in Figure 12 to show how the power gain behaves with respect to change of frequency, thus permitting an estimate of the bandwidth of emission. Note that in Figure 12 the range of frequency amplified

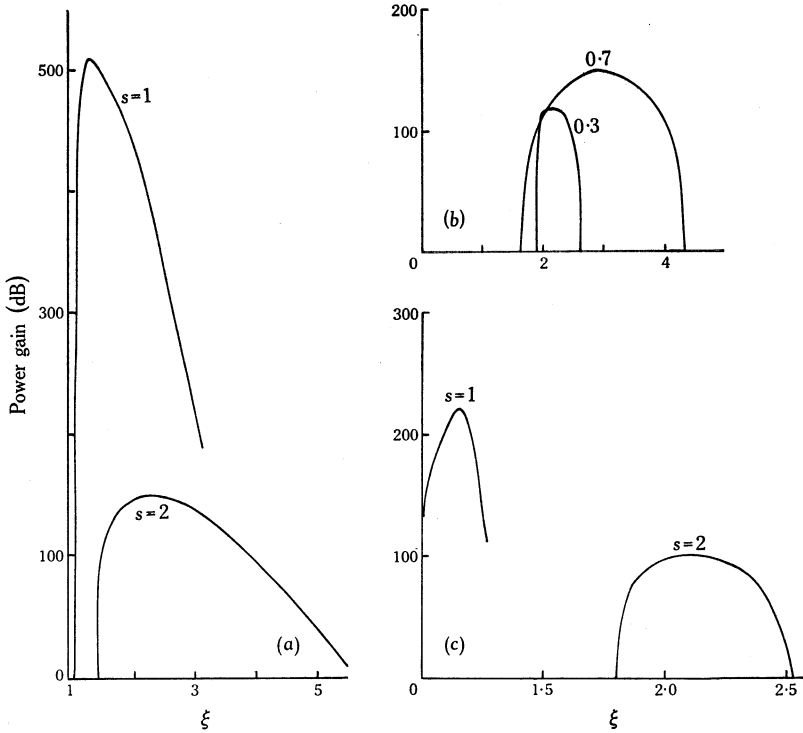


Fig. 12.—Power gain versus normalized wave frequency ξ for $f_H = 100$ Mc/s, $A = 1$, and
 (a) o-mode, $s = 1, 2$, $\beta_{\perp} = 0.1$, $\beta_{\parallel} = 0.7$, $\sigma = \omega_0^2/\omega_p^2 = 10^{-3}$, interaction time = 10^{-5} sec;
 (b) x-mode, $s = 2$, $\beta_{\perp} = 0.1$, $\beta_{\parallel} = 0.3, 0.7$, $\sigma = 10^{-3}$, interaction time = 10^{-5} sec;
 (c) o-mode, $s = 1, 2$, $\beta_{\perp} = 0.3$, $\beta_{\parallel} = 0.3$, $\sigma = 10^{-6}$, interaction time = 4×10^{-5} sec.

corresponds to different directions. However, if we consider a half-power or quarter-power emission cone and let the range of frequency radiated within this cone be the estimated bandwidth, then this bandwidth is the maximum that can be received on Earth, since the emission cone may be too wide and only part of the radiation will “strike” the Earth on account of the geometrical factor. Figure 12 shows that:

- (1) For both *single* and *double* types of frequency solutions, the bandwidth is small when the pitch angle is large.

- (2) When β_{\perp} and β_{\parallel} are fixed, the bandwidth for the *double* frequency solution is much narrower than that for the *single* frequency solution. Obviously, in this case, the harmonic number for the *single* frequency solution is one unit higher.
- (3) A bandwidth as narrow as $\Delta\xi \sim 0.09$ is possible. Note that in Figure 12 the pitch angle is 45° ; if the pitch angle is increased to greater than 60° , a half-power bandwidth of $\Delta\xi < 0.03$ is possible. Note also that the theoretical bandwidth decreases when the power gain is increased, i.e. allowing a longer interaction time or a denser stream.

(d) *Resonance Absorption at the First Three Harmonics*

It is well known from both classical and quantum theories that when an electron emits cyclotron radiation at some particular frequency it can also absorb radiation of the same frequency (e.g. Ginzburg 1964). When an electromagnetic wave passes through a magnetoactive plasma, some electrons respond to the wave gyrating at their own gyration frequency and either excitation or damping can take place, depending on the energy distribution of the electrons. Hence, whereas electromagnetic waves satisfying the resonance condition $\tilde{\omega} - k_{\parallel} v_{\parallel} - s\gamma\omega_H = 0$ will grow in a stream-plasma system (Section III(c)), they will be damped in a background plasma of "slow" electrons and ions (the resonance condition is now approximated to $\tilde{\omega} - s\omega_H \simeq 0$). Consequently, absorption will take place when an electromagnetic wave of angular frequency $\tilde{\omega}$, propagating in the active corona with varying magnetic fields in space, encounters angular gyrofrequency ω_H such that

$$\tilde{\omega} \simeq s\omega_H, \quad (3.12)$$

where $s = 1, 2, 3, \dots$. This type of collisionless absorption is called resonance absorption. It has been pointed out by Gershman (1960) that, since the collision frequency in the corona is very small ($\nu \sim 10^{-10}$), the only important absorption for transverse electromagnetic waves is the resonance absorption.

Let an electromagnetic wave be specified by $\exp i(kz - \omega t)$, where z is the direction along which the phase velocity is travelling. If we assume the frequency to be real and the wave vector complex, in order to look for a damping in space, we can write

$$k = \tilde{k} - iq$$

and the damping factor will be $\exp(-qz)$. According to Gershman (1960), the rate of the first harmonic absorption ($\omega \simeq \omega_H$) is given by

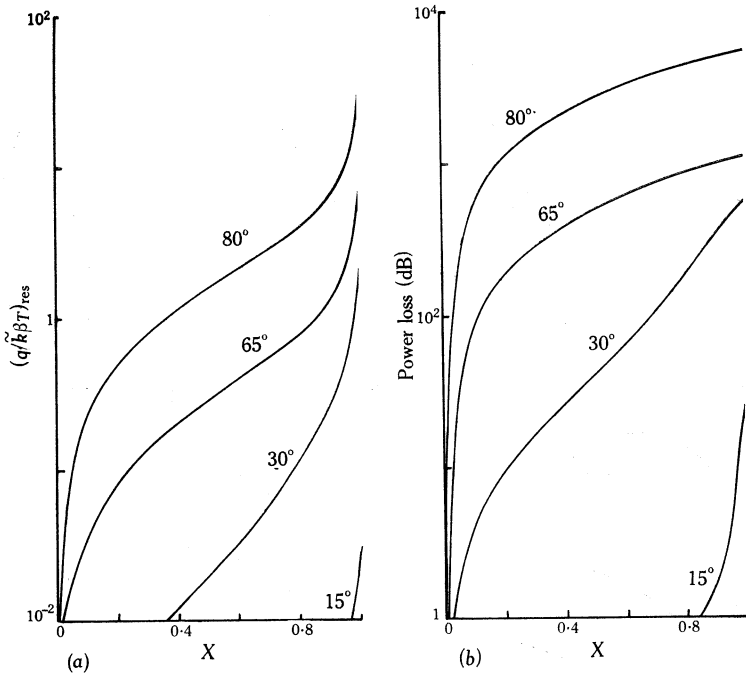
$$\begin{aligned} \left(\frac{q}{\tilde{k}}\right)_{s=1} &= \frac{(2/\pi)^{\frac{1}{2}}\beta_T \cos \theta/n_j X}{2X - 2 - \sin^2 \theta + 2n_j^2 \sin^2 \theta} \left[\left\{ 1 - \left(1 - \frac{7}{4} \sin^2 \theta\right) X \right\} n_j^4 \right. \\ &\quad - \left\{ 2 + X \left(-\frac{5}{2} + \frac{7}{4} \sin^2 \theta\right) + \frac{1}{4} X^2 (2 \cos 2\theta - \tan^2 \theta) \right\} n_j^2 \\ &\quad \left. + \left\{ 1 - \frac{3}{2} X + \frac{1}{2} X (1 - \tan^2 \theta) + \frac{1}{4} X^3 \tan^2 \theta \right\} \right], \quad (3.13) \end{aligned}$$

where $\beta_T = (\kappa T/m_0 c^2)^{\frac{1}{2}}$ is the normalized thermal velocity, κ is the Boltzmann constant, T is the temperature of the plasma in $^{\circ}\text{K}$, and $X = \omega_p^2/\omega^2$.

The width of the line $\omega \simeq \omega_H$ is of the order of

$$\Delta\omega \sim \omega \beta_T n_j \cos \theta = \omega(\kappa T/m_0)^{1/2} c n_j \cos \theta. \tag{3.14}$$

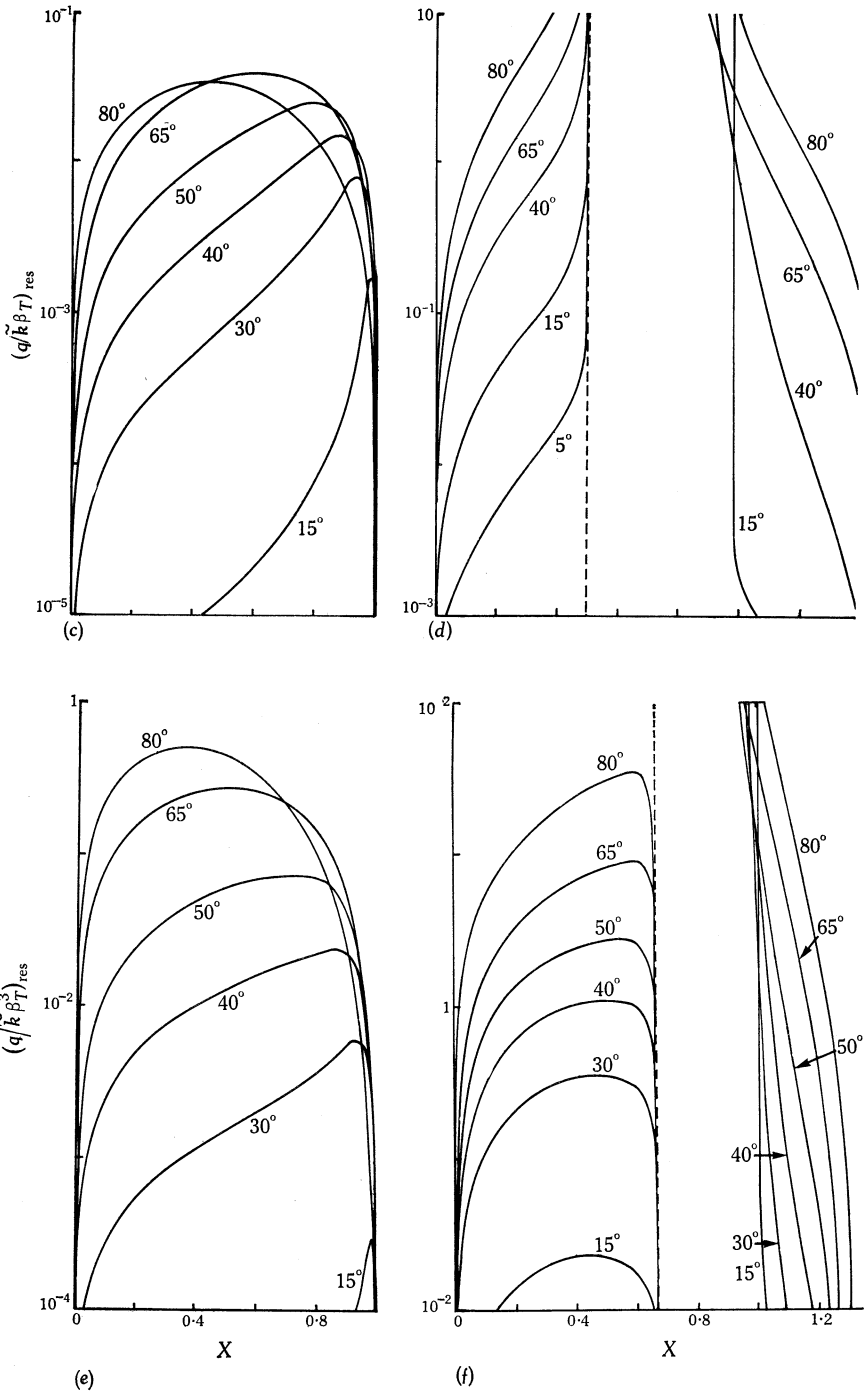
In studying the first harmonic absorption, we consider the absorption for the o-mode wave only, since an x-mode wave cannot escape through the level $X = 1 - Y$ if it passes through the level $Y = 1$ (here Y is defined by $Y = 1/\xi$). The dependence of the resonance specific absorption (specified by $q/(\tilde{k}\beta_T)$) for the first harmonic on the quantity X is shown in Figure 13(a) and the corresponding power loss in decibels is indicated in Figure 13(b), assuming the thickness of the absorption level $\Delta z = 10$ km.



Figs. 13(a) and 13(b).—Variation of (a) the resonance specific absorption $(q/(\tilde{k}\beta_T))_{res}$ and (b) the power loss, taking the thickness of the absorption layer to be 10 km and β_T to be 10^{-2} , with $X = \omega_p^2/\omega^2$ for the first harmonic in the o-mode and different values of the wave-normal angle θ in degrees.

In the graphs for power loss, the value of β_T is taken to be 10^{-2} (Gershman 1960) and the wave-normal angle θ is the parameter for each line. From these diagrams we observe that the absorption increases for increasing values of X and increasing wave-normal angle θ . We have seen in Section III(c) that, for cyclotron radiation caused by a gyrating electron stream with energy of the order of 100 keV per electron, a typical value of θ for maximum power (θ_m) in the case of the *double* frequency solution is 35° . With this value of θ , the resonance absorption is large except when X is small (say < 0.2 , Fig. 13(b)). This means that the source region for the o-mode radiation is limited to the region above the level $Y \simeq 1$.

The resonance specific absorptions for the second and third harmonics are given by Gershman (1960) and Ginzburg (1964) as



Figs. 13(c) to 13(f).—Variation of the resonance specific absorption $(q/\tilde{k}\beta_T)_{res}$ with $X = \omega_p^2/\omega^2$ for different values of the wave-normal angle θ in degrees; (c) second harmonic o-mode wave, (d) second harmonic x-mode wave, (e) third harmonic o-mode wave, (f) third harmonic x-mode wave.

$$\left(\frac{q}{\tilde{k}}\right)_{s=2} = \left(\frac{1}{2}\pi\right)^{\frac{1}{2}} V \exp\left(-\frac{(1-2\xi^{-1})^2}{2\beta_T^2 n_j^2 \cos^2 \theta}\right), \tag{3.15}$$

$$\left(\frac{q}{\tilde{k}}\right)_{s=3} = \left(\frac{1}{2}\pi\right)^{\frac{1}{2}} V \frac{3\beta_T^2 n_j^2 \sin^2 \theta}{8\xi^{-2}} \exp\left(-\frac{(1-3\xi^{-1})^2}{2\beta_T^2 n_j^2 \cos^2 \theta}\right), \tag{3.16}$$

where

$$V = \frac{X\beta_T n_j \xi \sin^2 \theta (\xi^{-1} - 1)/n_j^2}{2 \cos \theta [2(1 - \xi^{-1} - X + X\xi^{-1} \cos^2 \theta)n_j^2 - \{2(1 - X)^2 + (1 + \cos^2 \theta)X\xi^{-1} - 2\xi^{-1}\}]} \\ \times \left[\frac{1}{2}n_j^4 \sin^2 \theta + \left\{ X\left(\frac{1}{2} + \frac{\cos^2 \theta}{2} + \frac{\sin^2 \theta}{1 + \xi^{-1}}\right) - \frac{1}{2} \sin^2 \theta - 1 \right\} n_j^2 \right. \\ \left. + \left\{ \frac{X^2}{1 + \xi^{-1}} - X\left(\frac{1}{1 + \xi^{-1}} + 1\right) + 1 \right\} \right].$$

In calculating the second harmonic resonance absorption, we put $\xi = f/f_H = 2$ in (3.15), and substitute $\xi = 3$ in (3.16) for the third harmonic. Assuming $\theta \neq 0$, $\theta \neq \frac{1}{2}\pi$, $n_j \simeq 1$, we have the following rough estimations

$$\left. \begin{aligned} (q/\tilde{k})_{s=1} &\sim X\beta_T && \text{for the o-mode,} \\ (q/\tilde{k})_{s=2} &\sim X\beta_T && \text{for the x-mode,} \\ (q/\tilde{k})_{s=3} &\sim X\beta_T^3 && \text{for the x-mode.} \end{aligned} \right\} \tag{3.17}$$

For accurate calculation, we can use $q/\tilde{k}\beta_T$ and $q/\tilde{k}\beta_T^3$ to describe the second and third harmonic resonance specific absorption respectively. The relation between $q/\tilde{k}\beta_T$ and $X = \omega_p^2/\omega^2$ is shown in Figures 13(c) and 13(d) for the second harmonics of the o-mode and x-mode waves respectively. The corresponding graphs for the third harmonic, that is, $q/\tilde{k}\beta_T^3$ versus X , are given in Figures 13(e) and 13(f). Taking $\beta_T = 10^{-2}$, which is a typical value in the corona, and $z = 10$ km as the thickness of the absorption layer, one can calculate the power loss of an electromagnetic wave passing through the absorption level; such graphs are given in Figures 14(a) to 14(d), corresponding to Figures 13(c) to 13(f). In all these graphs, the parameter of each curve is the wave-normal angle θ . An inspection of Figures 13–14 indicates that the resonance specific absorption for the x-mode is at least two orders of magnitude higher than that for the o-mode and the corresponding power loss in decibels for the x-mode exceeds that for the o-mode by several orders of magnitude. In fact, Ginzburg and Zheleznyakov (1961) have already mentioned this result in a qualitative way. This is a very important fact concerning the escape conditions for the two modes and is referred to in the following section.

(e) Reflection Levels and Escape Conditions for the Two Characteristic Waves

It is well known from magnetoionic theory that the refractive index $n_j = 0$ at the level $X = 1 - Y$ for the x-mode for all θ , and at the level $X = 1$ for the o-mode for all values of θ except $\theta = 0^\circ$. One usually refers to the levels $X = 1 - Y$ and $X = 1$ as the reflection levels in a magnetoactive plasma; however, this is not always true. Jaeger and Westfold (1950) have shown that only a ray entering normally to the level $X = 1$ is reflected from this level and rays not normal to the stratification

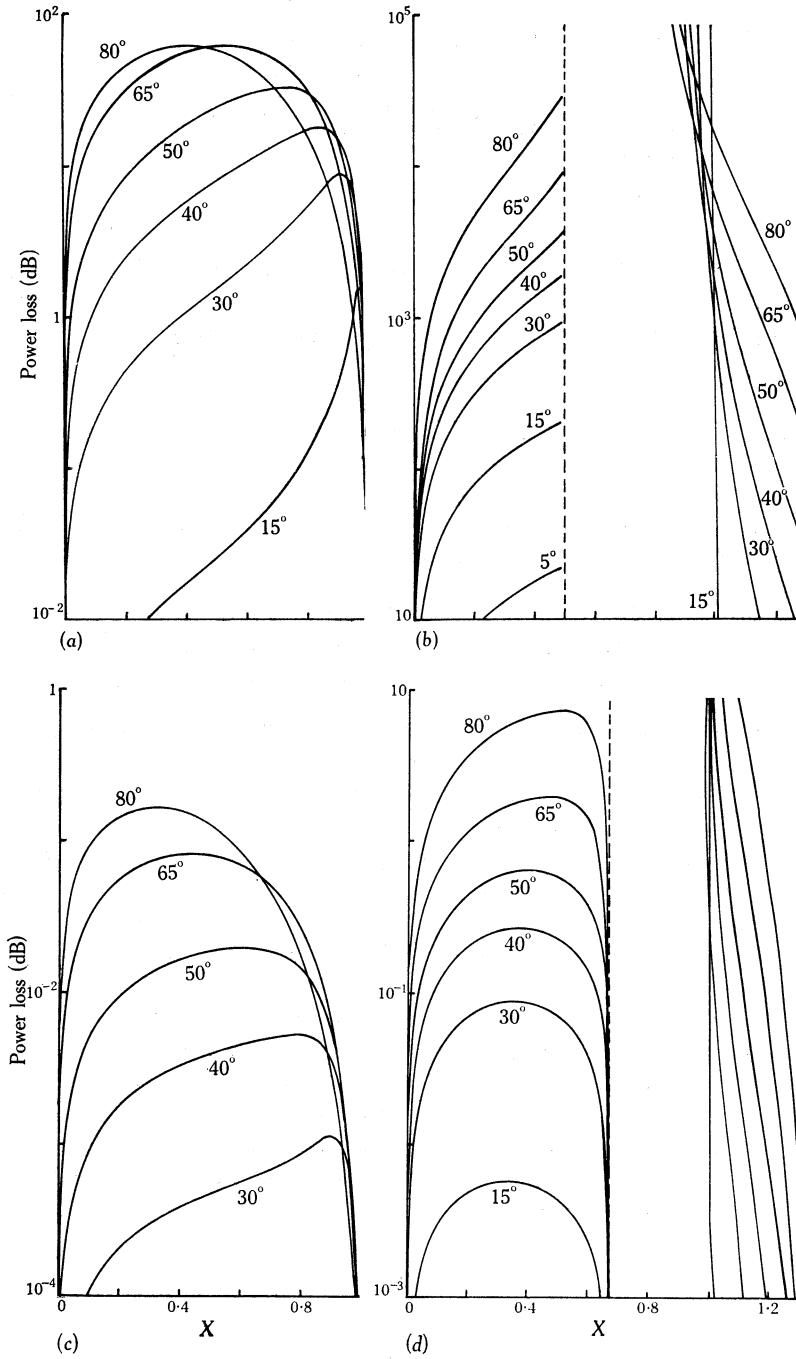


Fig. 14.—Variation of the power loss with $X = \omega_p^2/\omega^2$, taking the thickness of the absorption layer to be 10 km and β_T to be 10^{-2} , for different values of the wave-normal angle θ in degrees; (a) second harmonic o-mode wave, (b) second harmonic x-mode wave, (c) third harmonic o-mode wave, (d) third harmonic x-mode wave.

of refractive index are deviated according to Snell's law. In the solar atmosphere, where the electron density decreases radially and gradually, the reflection levels for large incident angles (with respect to the radius vector) will be shifted to higher altitudes where n_j is not zero. For a particular frequency, the reflection levels for both modes are, therefore, higher at the limb than near the centre of the solar disk. However, for a wave-normal direction not greater than about 35° with respect to the radius vector,* the levels corresponding to $n_j = 0$ can be assumed to be the true reflection levels and this assumption, unless otherwise stated, will be taken in the subsequent discussion of this section.

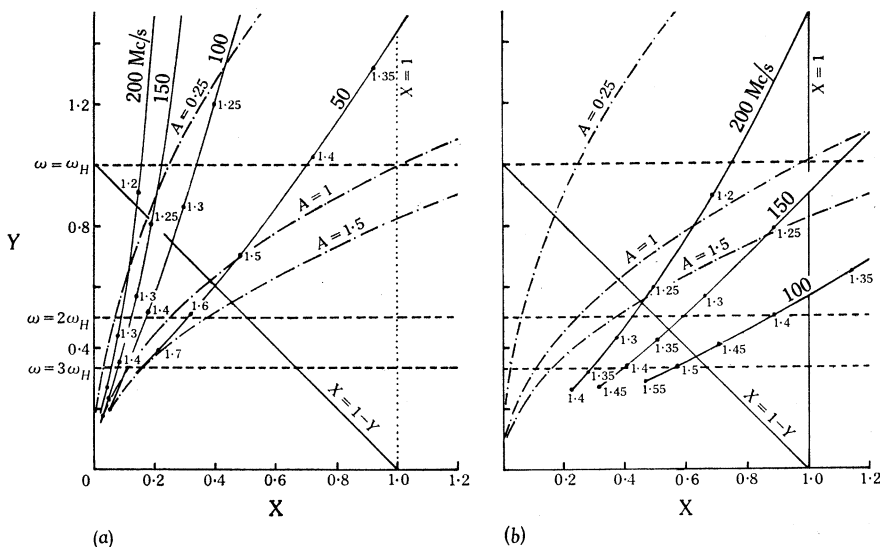


Fig. 15.—Relation between Y and X along the r -line of a unipolar spot specified by $H_s = 2000$ G for four frequencies, 200, 150, 100, and 50 Mc/s, when the electron density distribution follows (a) the Baumbach-Allen model and (b) the $5 \times$ Baumbach-Allen model; the numbers on the full curves show the position in units of solar radii. The horizontal dashed lines represent the three harmonic levels and the \cdots curves represent the identity $Y^2 = X/A$ for three values of A .

To study the escape conditions in the corona for the two characteristic waves, a conventional method is to relate, for a particular wave frequency, the quantities X and Y in graphical form (e.g. Pawsey and Bracewell 1955). We will discuss one such example below.

Suppose we take the maximum field intensity of the centre point on the spot surface of a unipolar spot field to be $H_s = 2000$ G, and we define the radial line passing through the said point to be the r -line. The magnetic field intensity of any point along this r -line will be given by (2.5). The radial variation of the plasma frequency is assumed to satisfy the Baumbach-Allen model (represented by Fig. 15(a)) or the $5 \times$ Baumbach-Allen model (represented by Fig. 15(b)). If we now consider a parti-

* It will be seen in another paper (Fung and Yip 1966) that in most cases the ray direction for frequencies of the order of 100 Mc/s differs from the wave direction only by a few degrees in the corona. We can therefore assume the two directions to be the same for such estimations.

cular electromagnetic wave with a certain wave frequency f , the values of X and Y along the r -line can be calculated with the help of Figure 2. In Figure 15 the full curves give the variation of X and Y along the r -line for four values of frequency, $f = 50, 100, 150, 200$ Mc/s. Each number on the curves indicates the value of $\rho = R/R_0$ at the particular point. The identity $Y^2 = X/A$ is shown in Figure 15 for three values of A (0.25, 1, 1.5). The first three harmonic levels ($Y = 1, \frac{1}{2}, \frac{1}{3}$) and the reflection levels ($X = 1, X = 1 - Y$) are also shown in the figure. We observe that as an electromagnetic wave of a particular frequency travels along the r -line it will first meet the o-mode reflection level and then, in succession, the first harmonic absorption level for the x-mode, the second harmonic absorption level, and the third harmonic absorption level. As this wave propagates, it encounters an increasing value of A . Considering propagation along the r -line, we can thus estimate the possible source positions for o- and x-mode waves from which the radio waves can escape. From Figure 15, we note that there is a much larger possible source region (in the square area bounded by $X = 1$ and $Y = 1$) from which an o-mode wave can escape without meeting the first harmonic absorption level and the reflection level, while an x-mode wave must be generated at a much higher level in order to avoid being reflected. In most cases, an escaping x-wave will have to encounter the second and third harmonic absorption levels, where the loss of energy is in general high.

So far, we have considered briefly the propagation along a field line of a unipolar spot only. It has been found in Section III(c) that the emission angle θ where maximum power occurs is not at $\theta = 0^\circ$ but ranges from 5° to 50° . A two-dimensional picture of the various reflection and absorption levels is needed when we consider radiation at the surface of a cone. Therefore, a more detailed discussion on the escape conditions for the two characteristic waves will be given below. We will take the example of a bipolar spot field; the argument is similar and simpler when a unipolar field is used instead.

After some tedious calculations, we show various levels of reflection and absorption for the frequencies 100, 150, and 200 Mc/s in Figures 16(a) to 16(c), where the electron density distribution in the active region is assumed to follow the $5 \times$ Baumbach-Allen or $10 \times$ Baumbach-Allen model and the value of H_s is taken to be 2500 G. The complete heavy loop shown in each of these diagrams is the strongest field line of the associated pair, and need not be the line passing through the centre of the spot area where H_s is specified.

Considering radiation from a helical stream, the result of investigations in Sections III(a) and III(c) indicates that when

$$A \simeq 1 \quad \text{or} \quad f_D \simeq f_H \quad (3.18)$$

the *double* frequency solution always exists for the o-mode in the fundamental harmonic radiation, which carries much more energy than any higher harmonic radiation ($s \geq 2$) in both the o- and x-modes. It has been pointed out that when the *double* frequency solution occurs the emission is in general narrow band. We may, therefore, consider the location specified by $A \simeq 1^*$ to be the best position where

* When A is greater than 1, the *double* frequency solution may still exist for a higher harmonic. In this case, the radiation power will be less. We should therefore keep in mind that the locality where $A \simeq 1$ is not the only location where bursts are radiated.

intense noise bursts are emitted. Moreover, the radiated frequency corresponding to maximum power for the *double* frequency solution at a source of local gyrofrequency f_H is always close to but greater than $f_H A^{\frac{1}{2}}$ (i.e. $\xi_m \geq A^{\frac{1}{2}}$, Sections III(a) and III(c)), that is

$$f \gtrsim f_H A^{\frac{1}{2}}. \quad (3.19)$$

Hence, from relations (3.18) and (3.19), the critical conditions for intense burst radiation at centre frequency f may be stated as

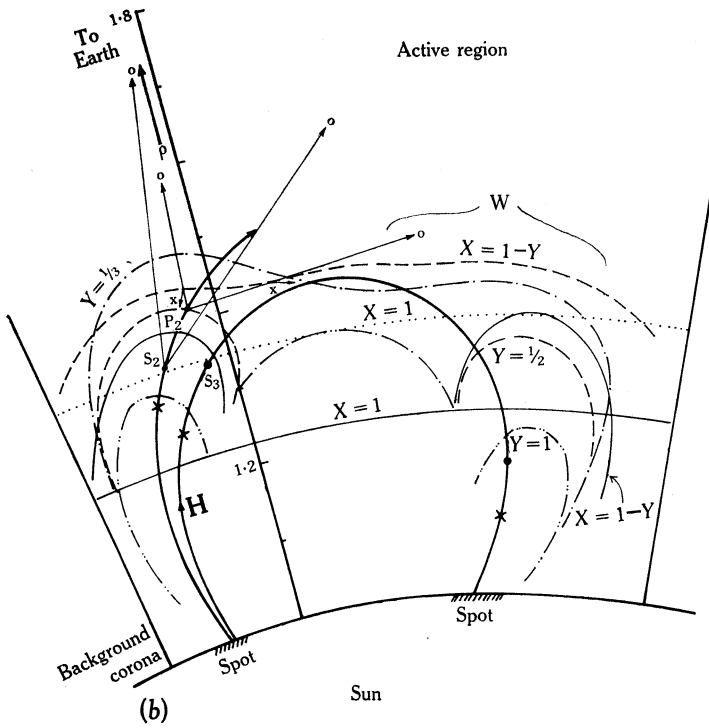
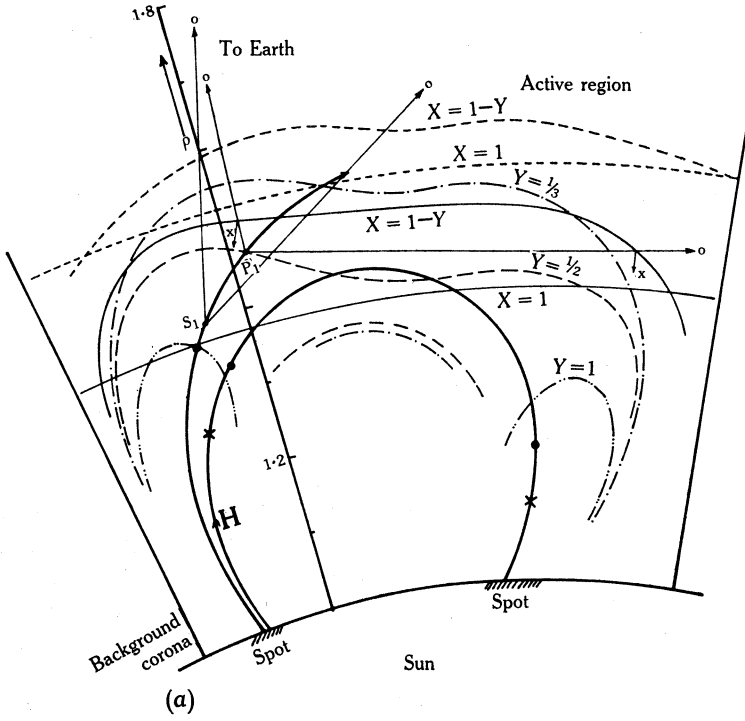
$$f_H \simeq f_D \lesssim f \quad (3.20)$$

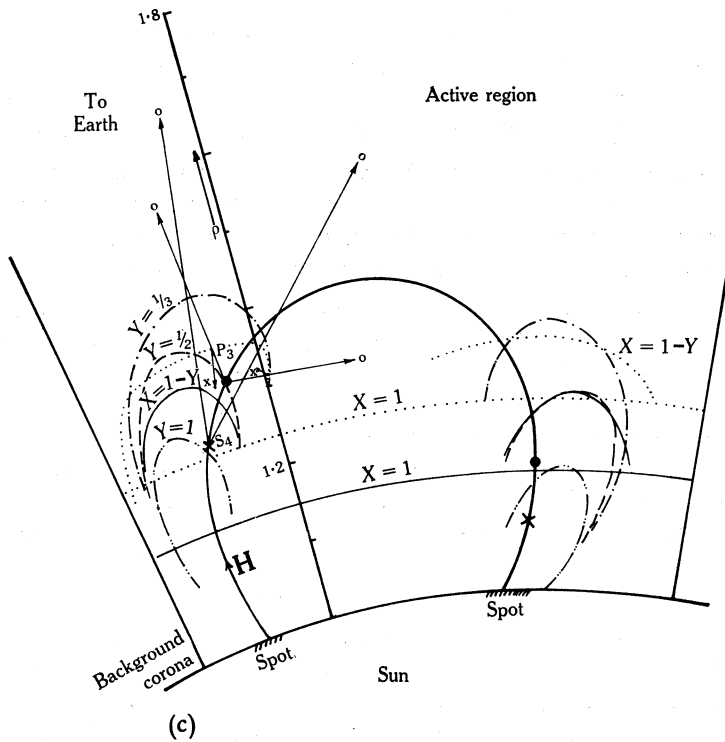
at the source. The conditions described by (3.20) may be referred to as the "intense burst radiation conditions".

An inspection of Figure 16(a) shows that for the $5 \times$ Baumbach–Allen model (full curves), a point like S_1 will satisfy the intense burst radiation conditions and the strong fundamental o-mode radiation, suffering some loss at the second harmonic absorption level and negligible loss at the third harmonic absorption level, will escape. It has been shown in Section III(a) that, in the possible source region, the lowest possible harmonic radiated in the x-mode is the second harmonic. Now the frequency corresponding to maximum power in the second harmonic is $f \simeq 2f_H$ (Section III(a)) for both the o- and x-modes. Consequently, to radiate a frequency of 100 Mc/s with significant power in the second harmonic, the source for both modes should be situated at the level where $f_H \simeq 50$ Mc/s. P_1 represents such a source in Figure 16(a) and it is seen that the x-mode waves will be reflected at the level $X = 1 - Y$, while the second harmonic o-mode emissions (responsible for the background continuum radiation) will escape. Referring to Figure 16(b) and taking the $10 \times$ Baumbach–Allen model of electron density distribution (broken curves), an electron stream gyrating through the point S_2 can readily radiate an intense noise burst of centre frequency 150 Mc/s. Using the $5 \times$ Baumbach–Allen model, S_3 could well be another possible burst source. Following the arguments as given above, x-mode waves of frequency 150 Mc/s radiated at P_2 will never be able to escape. In Figure 16(c), the intense burst radiation conditions are satisfied at a point like S_4 for the $10 \times$ Baumbach–Allen model. Radiating at P_3 , the x-mode waves again will be reflected. Note that even if the source for the second harmonic radiation is situated above the reflection level for the x-mode, the waves will have to pass through the third harmonic absorption level at which the value $X = A/9 \sim 0.25 - 0.5$ and the absorption for the x-mode is much higher than that for the o-mode (Figs. 13(e) and 13(f)). The result is that the second harmonic o-mode radiation will be predominant over the second harmonic x-mode emissions.

In Figure 16(b), consider the region (marked W) above the weaker spot of the bipolar group. Using the $10 \times$ Baumbach–Allen model of electron density distribution, since the level corresponding to $A = 1$ is well below both reflection levels, no significant radiation of any mode will escape the region above the weaker spot. This result holds generally for other frequencies.

The implications of all the important results shown in this section are summarized below.





Figs. 16(a) to 16(c).—Assuming $H_s = 2500$ G for the stronger spot of the associated pair, different levels of interest are shown in two dimensions for frequencies of (a) 100 Mc/s, (b) 150 Mc/s, and (c) 200 Mc/s; ——— for $Y = 1/3$, - - - - for $Y = 1/2$, — · — · — for $Y = 1$. The full curves for $X = 1$ and $X = 1 - Y$ are for a $5 \times$ Baumbach–Allen model of electron density distribution in the active region and the \bullet points represent the localities where $A = 1$. The broken curves for $X = 1$ and $X = 1 - Y$ are for a $10 \times$ Baumbach–Allen model and the \times points represent the localities where $A = 1$. The field lines are represented by the heavy arrowed curves, the complete loop indicating the strongest field line. Points S_1, S_2, S_3, S_4 are possible source positions where the intense burst radiation conditions are satisfied. P_1, P_2, P_3 represent the sources of second harmonic radiation in both modes. The thin straight arrows show the possible wave paths.

(f) Predictions of the Theory

If all theories, properties, and variables are taken into consideration in the study of escape conditions and the possible source positions for particular frequencies, the study and hence the discussion will be extremely complicated. In the above discussion we have only demonstrated one method by which the problem may be analysed. Investigation of many cases like the one just considered gives the following predictions from the theory of cyclotron radiation from electron streams.

- (1) In cases when the source is not too high, the second harmonic x-mode wave radiated is either reflected at the level $X = 1 - Y$ or suffers heavy loss of energy due to the third harmonic resonance absorption. The o-mode fundamental and second harmonic radiations, on the other hand, can be

excited readily by an electron stream gyrating at heights greater than the levels $X = 1$ and $Y = 1$. When the source is high enough, however, radiation in both modes may escape, but then the harmonic of radiation will be high (due to a large value of A) and the radiation power small. Hence, in general, only the o-mode radiation will assume significant power.

- (2) From Sections (a) and (c), the radiation power associated with the *double* frequency solution is much greater than the power of radiation for the *single* frequency solution. We suggest that radiation in the former case, in the o-mode, is the origin of storm burst phenomena.
- (3) If the *single* frequency solution is satisfied for the generating process, the bandwidth and emission cone are broad if the pitch angle of the stream is not too large. Since this case is always met with (whenever there is a *double* frequency solution there is always a *single* frequency solution with a greater harmonic number, whereas the reverse may not be true), many such events will occur simultaneously and all these broad-band emissions will superimpose to form a long-lived broad-band radiation—a type I background continuum. Fluctuations in plasma density and magnetic field will not result in any significant change in the superimposed radiation. Based on (1), the background continuum radiation is also in the o-mode.
- (4) In order to have intense storm bursts radiated in the o-mode near the centre of the solar disk, the electron density distribution needs to follow the $5 \times$ Baumbach–Allen or the $10 \times$ Baumbach–Allen model; in particular, the latter model is more favourable and all the following discussions will be based on this model.
- (5) No significant radiation will escape through the region above the weaker spot of the bipolar group in most cases when H_s (associated with the stronger spot) is less than about 3200 G. This result indicates that in the majority of cases the received radiation will be polarized in the o-mode with respect to the polarity of the stronger spot in the sunspot group.
- (6) From points (2) and (3) above, the background continuum radiation may not be able to survive absorption along the corona and be observed on the Earth. On the other hand, the *double* frequency solution is not always met with. As a result, storm bursts may be observed alone while at times continuum radiation may not be accompanied by storm bursts.
- (7) From Section (e), we observe that for a source near the centre of the solar disk, the source position of intense burst radiation at frequency f is always near and above the plasma level of this frequency.
- (8) For burst radiation in a particular spot-field configuration, the higher the emitted frequency (corresponding to maximum power) the lower the source position (Fig. 16).
- (9) The bandwidth of the superimposed broad-band radiation can be as high as several hundred Mc/s while the bandwidth of a narrow-band event can be as low as a few Mc/s.

IV. CONCLUSIONS

In this section we give a general picture of the proposed cyclotron theory and some concluding remarks in explanation of the noise storm phenomenon.

On the basis of the currently accepted theories (e.g. De Jaeger 1963; Wild, Smerd, and Weiss 1963), a flare, which results from the annihilation of a large volume of intense magnetic fields in the chromosphere or lower corona, gives rise to the production of high energy electrons and protons in different stages. At the first stage the explosion ejects charged particles in all directions, but the majority of the electrons (with energy of the order of 10–100 keV) are ejected along the neutral plane of a sunspot group. They travel in a radial direction and excite type III bursts (e.g. Kundu 1964). Some of the energetic electrons are trapped in the nearby magnetic fields and those particles arriving at a field line in about the same direction and with almost equal velocities will form an electron stream or bunch with a narrow momentum spread. When such a stream gyrates through the corona and whenever the *double* frequency solution is satisfied, a storm burst is radiated. The radiation power is strongest when the stream spirals through a region where the intense burst radiation conditions are satisfied. All the radiation from a number of streams satisfying the *single* frequency solution will superimpose to form a weak-intensity, wide-band, continuous radiation—the background continuum. With suitable geometrical conditions, the radiation will be observed on the Earth as a directly flare-related solar type I noise storm.

As mentioned in Section I, most noise storms are preceded by flares and the most probable delay is 30 min. It seems, therefore, that there is a lapse of time, approximately 30 min, during which either source electrons are as yet unavailable or that propagation conditions do not allow the radiated waves to escape. The flare phenomenon is very complex and is not well understood yet. From the more popular proposed theories of the flare evolution, it seems that the existence of trapped electrons with energies of the order of 10–100 keV in the source region after approximately 30 min of the initial explosive phase is possible (e.g. Kundu 1964). Noise storms will be radiated in the same manner in this case as described above.

The investigation in Section III(*f*) indicated that the intense burst radiation conditions are quite easily satisfied in the source region if the electron density is about 10 times the normal coronal background density. Working independently, this result on the magnitude of electron density agrees with the type II and type III radio observations of Weiss and others (Weiss 1963).

A comparison of the predictions of the cyclotron theory (Section III) with the observational data (Section I) shows that the mode of radiation, the narrow-band structure of storm bursts, the relation between the background continuum and storm bursts, the source positions of most storm bursts (concentrated near the centre of the solar disk), the association of noise storms with sunspots, and the relative angular sizes of storm bursts and background continuum are all well accounted for with our present theory. Based on the very limited knowledge of the flare phenomenon, the flare association property has been discussed in this section. There remain, however, three features that have not yet been discussed; these are the detailed dynamic

spectra of storm bursts, the polarization properties, and the estimation of electron density in the stream needed in order to account for the radio flux density received. The first feature will be considered in a subsequent paper where ray tracing in the solar corona is studied (Fung and Yip 1966) and the second feature has been discussed by Fung (1966*d*). We will consider the third feature below.

Assume that electrons in a volume of 100 m^3 of the stream radiate a particular frequency. Let N_0 be the density of the stream. The maximum power radiated by a single electron in the o-mode is about 10^{-21} W/sr . Then the total power associated with a particular frequency is about $10^{-19} N_0 G \text{ W/sr}$, where G is the power gain in the stream-plasma system. The theoretical flux density received on the Earth for a frequency of 100 Mc/s would then be $5 \times 10^{-50} N_0 G \text{ W m}^{-2} (\text{c/s})^{-1}$. Assuming the active region density to be 10^9 cm^{-3} and $\sigma = 10^{-6}$, giving $N_0 = 10^3 \text{ cm}^{-3}$, we have a theoretical flux density of approximately $5 \times 10^{-41} G$. Equating this value to the observed maximum flux density ($10^{-20} \text{ W m}^{-2} (\text{c/s})^{-1}$, e.g. Fokker 1960), we need a power gain of $G \sim 2 \times 10^{21}$ ($\sim 210 \text{ dB}$). We observe from Figure 11 that the interaction time needed is only about $4 \times 10^{-5} \text{ sec}$. The above estimation is very crude, but it seems that all the values involved are physically realizable.

V. ACKNOWLEDGMENTS

The authors are indebted to Professor G. R. A. Ellis, Physics Department, University of Tasmania, and to Dr. S. F. Smerd, Division of Radiophysics, CSIRO, Sydney, for critical reading of the manuscript and for very stimulating discussions.

VI. REFERENCES

- ALLEN, C. W. (1947).—*Mon. Not. R. astr. Soc.* **107**, 426.
 BRAY, R. J., and LOUGHHEAD, R. E. (1962).—*Aust. J. Phys.* **15**, 482.
 BRAY, R. J., and LOUGHHEAD, R. E. (1964).—"Sunspots." Ch. 5, Sect. 4. (Chapman & Hall: London.)
 DE JAEGER, C. (1963).—*Space Sci. Rev.* **1**, 487.
 DENISSE, J. F. (1959*a*).—Symp. IAU No. 9 (Paris 1958). p. 18.
 DENISSE, J. F. (1959*b*).—Symp. IAU No. 9 (Paris 1958). p. 237.
 EIDMAN, V. IA. (1958).—*Soviet Phys. JETP* **7**, 91.
 EIDMAN, V. IA. (1959).—*Soviet Phys. JETP* **9**, 947.
 ELGARROY, O. (1961).—*Astrophys. Norv.* **7**, 123.
 FUNG, P. C. W. (1966*a*).—*Planet. Space Sci.* **14**, 335.
 FUNG, P. C. W. (1966*b*).—*Planet. Space Sci.* **14**, 469.
 FUNG, P. C. W. (1966*c*).—*Aust. J. Phys.* **19**, 489.
 FUNG, P. C. W. (1966*d*).—Ph.D. Thesis, Univ. Tasmania.
 FUNG, P. C. W., and YIP, W. K. (1966).—*Planet. Space Sci.* (In press.)
 GERSHMAN, B. N. (1960).—*Soviet Phys. JETP* **11**, 657.
 GINZBURG, V. L. (1964).—"The Propagation of Electromagnetic Waves in Plasma." (Pergamon Press: New York.)
 GINZBURG, V. L., and ZHELEZNYAKOV, V. V. (1959).—*Soviet Astr. AJ* **3**, 235.
 GINZBURG, V. L., and ZHELEZNYAKOV, V. V. (1961).—*Soviet Astr. AJ* **5**, 1.
 GOLDSTEIN, S. J., JR. (1959).—*Astrophys. J.* **130**, 393.
 HEY, J. S. (1946).—*Nature, Lond.* **157**, 47.
 JAEGER, J. C., and WESTFOLD, K. C. (1950).—*Aust. J. scient. Res. A* **3**, 376.
 KAI, K. (1962).—*Publs astr. Soc. Japan* **14**, 1.
 KIEPENHEUER, K. O. (1946).—*Nature, Lond.* **158**, 340.

- KRUSE, U. W., MARSHALL, L., and PLATT, J. R. (1956).—*Astrophys. J.* **124**, 601.
- KUNDU, M. R. (1964).—Solar radio astronomy. Vol. 2, Rep. No. 64-4, Radio Astronomy Observatory, Univ. Michigan.
- LIEMOHN, H. B. (1965).—*Radio Sci.* **69D**, 741.
- MALINGE, A. M. (1963).—*Annls Astrophys.* **26**, 97.
- MARTYN, D. F. (1946).—*Nature, Lond.* **158**, 632.
- MORIMOTO, M., and KAI, K. (1961).—*Publs astr. Soc. Japan* **13**, 294.
- NEWKIRK, G. (1959).—Symp. IAU No. 9 (Paris 1958). p. 149.
- PAWSEY, J. L. (1950).—*Proc. Instn elect. Engrs* (3) **97**, 290.
- PAWSEY, J. L., and BRACEWELL, R. N. (1955).—"Radio Astronomy." (Clarendon Press: New York.)
- PAYNE-SCOTT, R., and LITTLE, A. G. (1951).—*Aust. J. scient. Res. A* **4**, 508.
- PAYNE-SCOTT, R., YABSLEY, D. E., and BOLTON, J. G. (1947).—*Nature, Lond.* **160**, 256.
- SHAIN, C. A., and HIGGINS, C. S. (1959).—*Aust. J. Phys.* **12**, 357.
- SUZUKI, S. (1961).—*Ann. Tokyo astr. Obs.* (2) **7**, 75.
- TAKAKURA, T. (1956).—*Publs astr. Soc. Japan* **8**, 182.
- TAKAKURA, T. (1961).—*Publs astr. Soc. Japan* **13**, 166.
- TAKAKURA, T. (1963).—*Publs astr. Soc. Japan* **15**, 462.
- TCHICHACHEV, B. M. (1956).—5th Colloquium on Cosmogony, Moscow, p. 245.
- TWISS, R. Q., and ROBERTS, J. A. (1958).—*Aust. J. Phys.* **11**, 424.
- VITKEVICH, V. V., and GORELOVA, M. V. (1961).—*Soviet Astr. AJ* **4**, 595.
- WEISS, A. A. (1963).—*Aust. J. Phys.* **16**, 240.
- WILD, J. P. (1951).—*Aust. J. scient. Res. A* **4**, 36.
- WILD, J. P., and SHERIDAN, K. V. (1958).—*Proc. Instn Radio Engrs* **46**, 160.
- WILD, J. P., SMERD, S. F., and WEISS, A. A. (1963).—*Ann. Rev. Astron. Astrophys.* **1**, 291.

